

Response of organic aerosol to Delhi's pollution control measures over the period 2011–2018

James M. Cash^{a,b,*}, Chiara Di Marco^a, Ben Langford^a, Mathew R. Heal^b, Tuhin K. Mandal^c, Sudhir K. Sharma^c, Bhola Ram Gurjar^d, Eiko Nemitz^{a,**}

^a UK Centre for Ecology & Hydrology, Edinburgh Research Station, Penicuik, EH26 0QB, UK

^b School of Chemistry, University of Edinburgh, Edinburgh, EH9 3FJ, UK

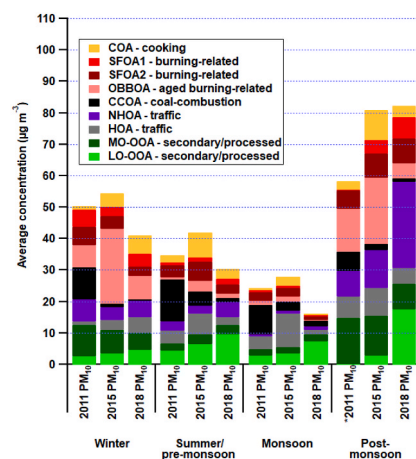
^c CSIR-National Physical Laboratory, Dr. K S Krishnan Road, New Delhi, 110012, India

^d Department of Civil Engineering, Indian Institute of Technology Roorkee, India

HIGHLIGHTS

- A novel offline aerosol mass spectrometry method has been developed.
- Burning-related OA was the largest contributor during peak PM concentrations.
- Despite a ban, open waste and crop-residue burning were active in 2018.
- Coal power station closures and coal-use reductions likely decreased OA.
- Heavy goods vehicles restrictions may inadvertently cause increases in OA.

GRAPHICAL ABSTRACT



ARTICLE INFO

Keywords:

Particulate matter
Organic aerosol
Offline aerosol mass spectrometry
Positive matrix factorisation
Delhi
Source apportionment

ABSTRACT

Some of the world's highest air pollution episodes occur in Delhi, India and studies have shown particulate matter (PM) is the leading air pollutant to cause adverse health effects on Delhi's population. It is therefore vital to chart sources of PM over long time periods to effectively identify trends, particularly as multiple air quality mitigation measures have been implemented in Delhi over the past 10 years but remain unevaluated. An automated offline aerosol mass spectrometry (AMS) method has been developed which has enabled high-throughput analysis of PM filters. This novel offline-AMS method uses an organic solvent mix of acetone and water to deliver high extraction recoveries of organic aerosol (OA) ($95.4 \pm 8.3\%$). Positive matrix factorisation (PMF) source apportionment was performed on the OA fraction extracted from PM₁₀ filter samples collected in Delhi in 2011, 2015 and 2018 to provide snapshots of the responses of OA to changes in sources in Delhi. The

* Corresponding author. The James Hutton Institute, Craigiebuckler, Aberdeen, AB15 8QH, UK.

** Corresponding author. UK Centre for Ecology & Hydrology, Edinburgh Research Station, Penicuik, EH26 0QB, UK.

E-mail addresses: James.Cash@hutton.ac.uk (J.M. Cash), en@ceh.ac.uk (E. Nemitz).

<https://doi.org/10.1016/j.atmosenv.2023.120123>

Received 27 April 2023; Received in revised form 14 September 2023; Accepted 1 October 2023

Available online 3 October 2023

1352-2310/© 2023 The Authors. Published by Elsevier Ltd. This is an open access article under the CC BY license (<http://creativecommons.org/licenses/by/4.0/>).

nine factors of OA resolved by PMF group into four primary source categories: traffic, cooking, coal-combustion and burning-related (solid fuel or open burning). Burning-related OA made the largest contribution during the winter and post-monsoon, when total OA concentrations were at their highest. Annual mean burning-related OA concentrations declined by 47% between 2015 and 2018, likely associated with the 2015 ban on open waste burning and controls and incentives to reduce crop-residue burning. Compositional analysis of OA factors shows municipal waste burning tracers still present in 2018, indicating further scope to reduce burning-related OA. The closure of the two coal power stations, along with initiatives to decrease coal use in industry, businesses, and residential homes, resulted in a significant decrease (87%) in coal-combustion OA. This corresponds to a 17% reduction in total OA, which shows the effectiveness of these measures in reducing PM₁₀. Increases in traffic OA appear to have been offset by the introduction of the Bharat stage emissions standards for vehicles as the increases do not reflect the rapid increase in registered vehicles. However, daytime restrictions on heavy goods vehicles (HGVs) entering the city is linked to large increases in PM₁₀ during the winter and post-monsoon, likely because the large influx of diesel-engine HGVs during the early mornings and evenings is timed with a particularly low planetary boundary layer height that enhances surface concentrations.

1. Introduction

Air pollution is one of India's biggest health problems. Over the past decade, there has been an increasing fossil fuels demand due to rapid growth in industry, registered vehicles and population (Gulia et al., 2022). Electricity demands have also increased and the majority (~60%) is generated through coal-fired thermal power stations (Yang and Urpelainen, 2019). This, combined with widespread open burning of municipal waste and crop-residue, results in particularly poor air quality. Estimates for 2019 suggest 17.8% of premature deaths in India can be attributed to air pollution with 10.4% due to ambient particulate matter (PM) (Pandey et al., 2021). One of the most polluted cities in India is Delhi, which is a densely populated megacity with over 31.2 million inhabitants (Sharma et al., 2021), and in which PM concentrations frequently exceed World Health Organization (WHO) guideline concentrations (Sharma et al., 2018). The characterization of the sources of PM is therefore critical for development of air quality mitigation strategies.

Aerosol Mass Spectrometry (AMS) has been used for two decades to quantify PM₁ chemical composition (DeCarlo et al., 2006; Hunt and Petrucci, 2002), but the instruments are costly to deploy and require specialist knowledge to operate in the field. As a result, measurement campaigns are generally short, particularly when using high-resolution time-of-flight AMS (HR-TOF-AMS) and data prior to 2017 are very limited. There is a particular paucity of AMS measurements conducted in India. A recent development has been HR-TOF-AMS measurements on resuspended airstreams of PM filter samples (offline-AMS) (Bozzetti et al., 2017; Daellenbach et al., 2016, 2017). This enables high-resolution chemical analysis of PM without the additional cost of HR-TOF-AMS field deployment. Research institutes and statutory monitoring bodies often store filter archives to be reanalysed which creates the opportunity to characterize PM from the past, and the present, using one technique.

The current offline-AMS methods focus on using water as the extracting solvent which limits the fraction of the organic aerosol (OA) component that can be extracted from PM filter samples, particularly as the majority of studies report that water-insoluble OA (WIOA) contributes between 10 and 84% of total OA (Ge et al., 2017; Jayarathne et al., 2018; Li et al., 2015; Saarikoski et al., 2008; Sun et al., 2011; Ye et al., 2017). The amount of WIOA is accentuated by the primary organic aerosol (POA) content which originates from sources such as traffic and cooking for which recovery by water extraction is particularly low (Daellenbach et al., 2016). This is an issue when measuring PM in places with high primary emissions of OA. Since previous studies have shown this to be the case in Delhi (Cash et al., 2021; Reyes-Villegas et al., 2020), we have developed an offline-AMS method that uses an organic solvent mix to extract OA from PM filter samples. The following potential issues arise with using organic solvents in offline-AMS (Bozzetti et al., 2017):

1. The potential for the solvent to cause a high AMS organics background and
2. The potential for the solvent to interact or react with the extracted sample organics.

Previous studies using organic solvents to extract PM from filters have shown a reduction in the organics background after using activated-carbon-filled diffusion dryers (Chen et al., 2016; Han et al., 2016; Mihara and Mochida, 2011). For example, Mihara and Mochida (2011) reported good agreement between mass spectra measured using deuterated or non-deuterated methanol and ethyl acetate solvents to extract PM from filters, even after leaving the samples for 1 week at room temperature. This suggests organic solvents offer high stability (i. e. resistance to compositional change due to chemical reaction) and the possibility of an offline-AMS method with minimal contamination from the solvent.

Over the last 20 years, a series of mitigation strategies have been implemented in Delhi to curb the high concentrations of air pollutants (Table 1). A number of vehicle emissions and fuel standards (Bharat stages) were implemented in 2000, 2005, 2010 and 2018 (Gulia et al., 2018). These have gradually decreased the tailpipe emissions of vehicles in Delhi (and other metro cities). The first strategy to have a

Table 1

Air quality mitigation strategies implemented in Delhi over the last 20 years. The table is adapted from that presented in Gulia et al. (2018).

Mitigation strategy	Year	Sources or areas controlled
Bharat stage I	2000	All vehicles
Bharat stage II	2000	Initially in metro cities (including Delhi)
Public transport vehicles moved from diesel to compressed natural gas (CNG) engines	2001	Public transport
Bharat stage III	2005	Initially only in national capital region (NCR – Delhi included)
Bharat stage IV	2010	Initially only in NCR
Heavy goods vehicle (HGV) restrictions (7:00 a.m.–10:00 p.m.)	2014	HGVs
Ban on open waste burning	2015	Residents of Delhi
Shutdown of the Rajghat thermal power station	2015	Located in the east of New Delhi
Ban on >2000 cc diesel-engine vehicles	2016	Luxury diesel vehicles
No entry for HGVs in NH-2, 10 and 58 area codes	2016	HGVs
Odd-even car scheme	2016	Cars
Deregistration of diesel vehicles older than 10 years or more	2016	Diesel vehicles
Ban on crop-residue burning	2016	Neighbouring states of Uttar Pradesh, Haryana, Punjab, Rajasthan
Bharat stage VI	2018	NCR
Shutdown of the Badarpur thermal power station	2018	Located in the southeast district of Delhi

demonstrable effect on air quality was the shift in 2001 from diesel-engine public transport vehicles to compressed natural gas (CNG) fuelled vehicles (Kathuria, 2005; Krelling and Badami, 2022). However, the observed decrease in PM₁₀ concentrations in 2001 and 2002 was short-lived as the increase in registered vehicles subsequently led to increased concentrations (Sindhwani and Goyal, 2014). There were 6.35 million registered vehicles in 2011, rising to 8.29 million in 2014, and to more than 11 million in 2020 (Jain et al., 2020). Further diesel-related mitigation strategies were therefore implemented. In 2014, time restrictions (7:00 a.m.–10:00 p.m.) were put in place for heavy goods vehicles (HGV) entering the city in order to reduce congestion and midday peaks in traffic emissions. In 2015, there was a ban on open waste burning as studies started to suggest this produced significant air pollutant concentrations (Gulia et al., 2018). In 2016, there was a ban on luxury diesel vehicles (engines >2000 cc) and on diesel vehicles 10 years or older, and a complete ban on HGVs in certain areas of Delhi (Gulia et al., 2018). Also in 2016, a scheme was designed to restrict the number of cars entering the city according to whether the vehicle number plate begins with an odd or even number. This “Odd-even scheme” has been evaluated as an “unsuccessful” mitigation measure (Chowdhury et al., 2017) causing only a small decrease in air pollutants (Sharma et al., 2017).

Some of these strategies are untested for their efficacy and, to our knowledge, the majority of evaluations have been confined to total PM₁₀ mass-based measurements (Kathuria, 2005), global satellite observations (Chowdhury et al., 2017) or model simulations (Gulia et al., 2018, 2022; Sindhwani and Goyal, 2014) which do not provide a robust measurement-based link between changes in concentration and in emissions from specific sectors. A more detailed analysis of the historic sources of PM₁₀ would improve evaluation of past mitigation

implementations. Consequently, in this work, we apply a high-throughput offline-AMS analysis protocol to analyse PM samples collected over multiple years and use this to track the contribution of different sources via source apportionment analysis of the organic fraction. The results are used to chart the extent to which mitigation strategies are associated with changes in PM from the intended sources.

2. Methods

2.1. Filter sample collection

Filter samples were collected at a 10 m height at the CSIR-National Physical Laboratory (CSIR-NPL) situated west of central New Delhi (28°38' N, 77°10' E) (Fig. 1). The CSIR-NPL campus is surrounded by agricultural fields in the northwest and southwest (~1.5 km), managed by the Indian Agriculture Research Institute. There are busy roads ~100 m to the north, northwest and west, along with green parks and forests ~1.2 km to the south. The large Lohamandi and Mayapuri industrial areas are situated ~5 km to the southwest. There are large residential and commercial areas to the northwest (Kirti Nagar, ~3 km), north (Patel Nagar, ~1 km) and northeast (Karol Bagh, ~1 km). There are also two nearby thermal power stations: The Rajghat thermal power station (~8 km east) and the Badarpur thermal power station (~20 km southeast).

Filter samples analysed here were collected from January until December for the years of 2011 ($n = 50$), 2015 ($n = 113$) and 2018 ($n = 80$). In 2011, the filters were sampled 4–5 times a month on an 8 h basis every Wednesday, during the morning (10:00 to 18:00 h) and night (18:00 to 02:00 h), using a Respirable Dust Sampler (Model: PEM-RDS 8NL, S/No.:1709; Make: M/s. Polltech Instruments, Mumbai, India).

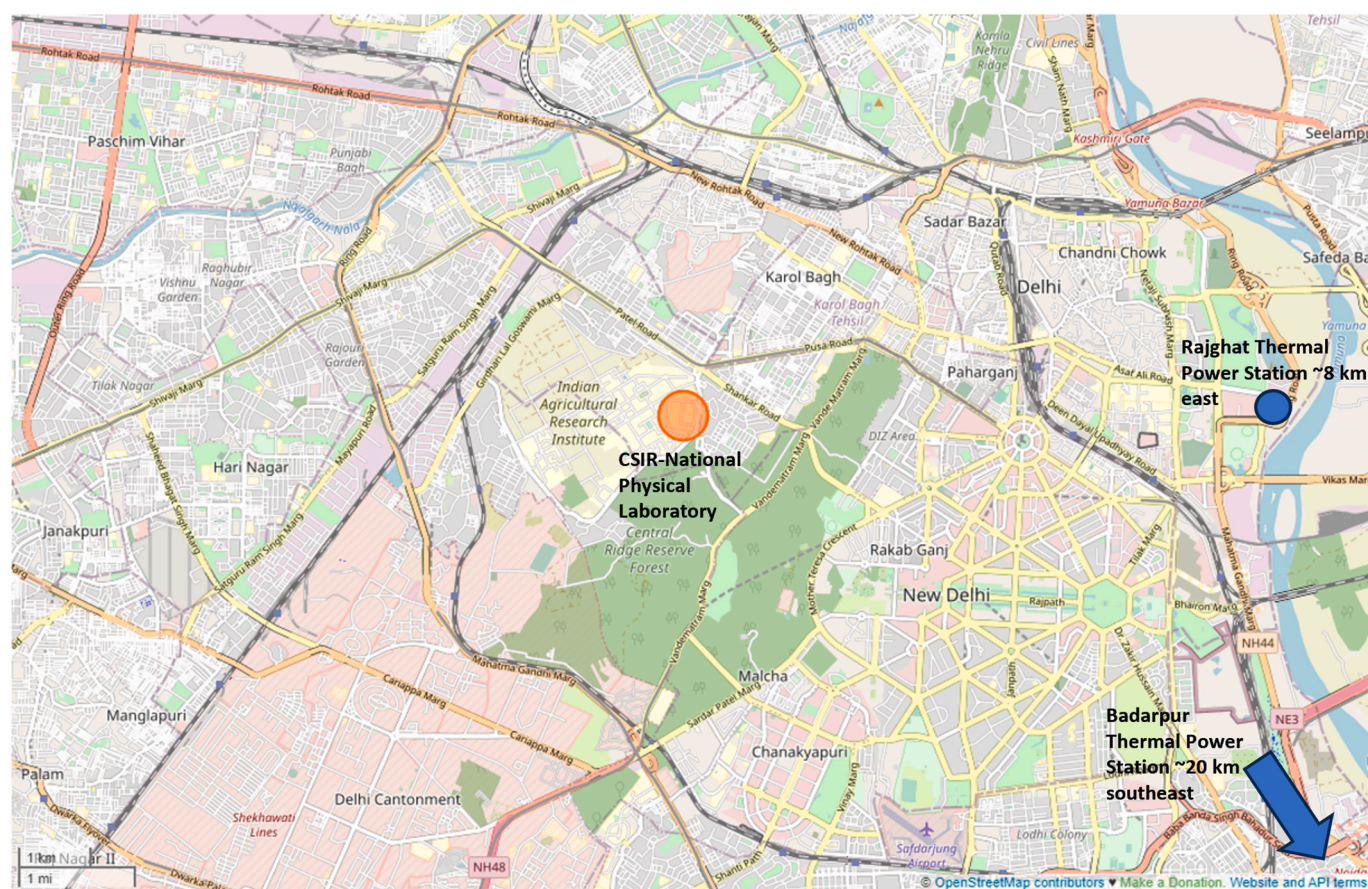


Fig. 1. Map of New Delhi showing the area surrounding the measurement site (marked with an orange circle) along with labels showing the position of the Rajghat thermal power station (blue circle) and a blue arrow indicating the direction of the Badarpur thermal power station.

For 2015; 2018, the filters were sampled over 24 h (10:00 to 10:00 h) with at least two filters being sampled per week (weekdays and weekends included to reduce the day-of-the-week effect) using a Respirable Dust Sampler (Model: AAS-217 NL; Make: M/s. Ecotech, Delhi, India). The quartz fibre filters (QM-A) were prebaked (550 °C for 6 h) before sampling at a flow rate of 1.2 m³ min⁻¹ with ±2% accuracy. The filters were stored at -20 °C before analysis. More information on the sampling method is described in previous studies (Banoo et al., 2020; Jain et al., 2020; Sharma et al., 2014, 2021).

The difference in the sampling schedule in 2011 compared to 2015 and 2018 may have allowed the PMF model to separate factors based on intraday variability. This could cause factors to be separated for 2011 that do not exist in 2015 and 2018; however, we did not find this to be the case and therefore we did not combine samples to represent daily measurements. The PMF factors that resulted were consistent with those seen before in Delhi.

For data analysis, the year is split into four seasons: winter (January–February), pre-monsoon/summer (March–May), monsoon (June–September) and post-monsoon (October–December). The seasonal averages of temperature and relative humidity are summarised in Fig. 2. Half hourly temperatures decrease to a minimum of ~3 °C in winter, with peak temperatures of ~47 °C in summer. The monsoon is characterised by large rainfall events during which relative humidity is high compared to its adjacent seasons (monsoon average ~ 70%). The post-monsoon and winter seasons exhibit dramatic changes in the diurnal planetary boundary layer height caused by sharp changes in temperature between the day and night. The contraction in the boundary layer during the night causes near-surface pollutant concentrations to increase significantly. As temperatures drop further in the winter, severe fog and haze events cause reduced visibility.

2.2. Offline-AMS

A new fully-automated sampling system to perform high-throughput analysis of filter extracts was developed for this study (Figure S1, supplementary information (SI) Section S1). Filter punches of area 2 cm² were first extracted in a solvent (5 mL) and ultrasonicated for 20 min at 30 °C. A range of solvents were assessed, and the final solvent mix chosen to extract the filter samples was 1:1 acetone (99.8%, HPLC grade, Thermo Scientific™) to ultrapure water (18.2 MΩ cm, total organic carbon (TOC) < 5 ppb, 25 °C). Details on how this solvent was chosen are provided in SI section S2. The extracts were then filtered (0.45 μm pore size) before being placed in an autosampler for injection of samples into a tailor-made nebuliser and aerosolisation using compressed argon. The generated particles filled a PTFE spray chamber and excess liquid fell into a separate beaker. The chamber was fitted with a pressure

sensor to ensure consistent aerosol production. The aerosol was then dried through a series of dryers which differed according to the solvent. A Perma Pure Nafion™ membrane dryer (model: MD-070, Perma Pure LLC) was used for removal of water from the airstream. For organic solvent removal, diffusion dryers filled with activated carbon were used along with a tailor-made gas-phase denuder filled with activated carbon monolith.

The dried aerosol stream passed through to the inlet of a high-resolution time-of-flight aerosol-mass-spectrometer (HR-TOF-AMS, Aerodyne Research Inc.). The HR-TOF-AMS was operated in V-mode and further operational details and descriptions of the instrument can be found elsewhere (Canagaratna et al., 2007; DeCarlo et al., 2006). In summary, particles pass through a ~PM₁ aerodynamic lens into the particle sizing time-of-flight chamber. Here, a chopper wheel controls the particle beam entering the chamber. Once sized, particles collide with a thermal vaporisation plate (600 °C) and the resultant non-refractory species are ionised (70 eV). The ions are propelled by a pulser into the time-of-flight *m/z* analyser before being detected. The measured signal is the difference between the signal measured when the chopper is closed (background spectrum) and open in order to remove background effects. Each filter extract was measured for a total of 5 min at one difference spectrum (= chopper open – chopper closed) per 15 s. This high measurement frequency allowed for anomalies in the aerosol stream to be removed from the 5-min averaged spectra.

In between each sample run, an automated 7-min wash cycle was performed where ultrapure water (18.2 MΩ cm, total organic carbon (TOC) < 5 ppb, 25 °C) was injected into the sampling system. Samples of the solvent used for extraction were frequently included in the sample carousel. The solvent spectra and wash cycle spectra were subtracted from the final measurement to reduce memory effects. A typical sample run of AMS measured concentrations of nebuliser generated PM is shown in Figure S2. Detailed investigations into the possible effects of the extracting solvent on the offline-AMS measurements, along with an estimate of the OA recovery, are described in SI Section S3.

A total of 2078 ions (including isotopes) were fitted (*m/z* 12–328) and analysed in SQUIRREL (Sequential Igor data Retrieval) v1.64 and PIKA (Peak Integration by Key Analysis) v1.24 which are coded in IGOR Pro (WaveMetrics, Inc., Portland, OR, USA). Peaks were fitted based on an improvement of the open and closed spectrum residual signals rather than using the difference spectrum residuals as this can cause ambiguity. Peaks were omitted if their average signal was less than 10 Hz ns⁻¹.

Argon was used as the airbeam correction within SQUIRREL and, given the argon atmosphere, the CO⁺ peak (*m/z* 28) was fitted explicitly, rather than assumed to be equal to the signal at of CO₂⁺, which is standard practise for ambient AMS analysis where the peak at *m/z* 28 is swamped by N₂⁺. An increase in CO₂⁺ was also observed when nebulising

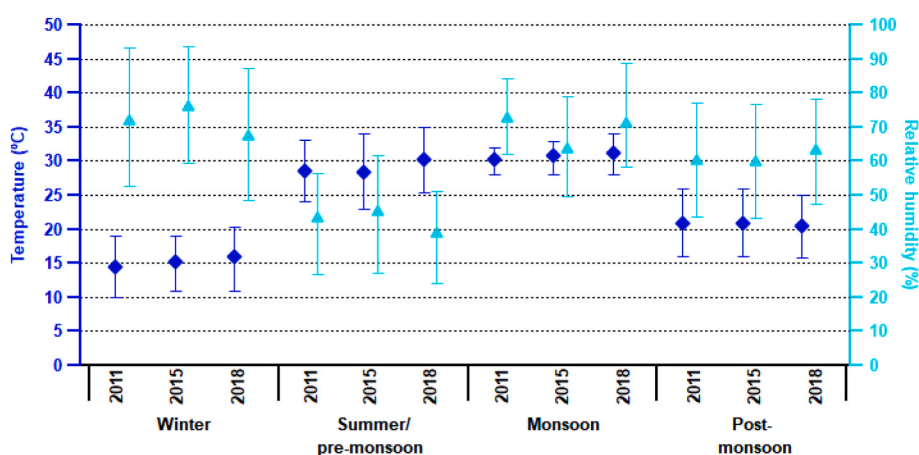


Fig. 2. Seasonal average temperature (blue diamonds) and relative humidity (cyan triangles) for the years of 2011, 2015 and 2018. The bars show the 25th and 75th interquartile range of the underlying hourly data. Values shown are an average across the entire season.

pure NH_4NO_3 which has previously been shown to be due to surface ionisation of organics within the instrument (Pieber et al., 2016). This arises from thermal decomposition reactions of NH_4NO_3 particles colliding with charred organic residue left on the particle vaporizer or ion chamber. The corrected CO_2^+ signal, $\text{CO}_{2,\text{corr}}$, was calculated using the relationship (Pieber et al., 2016):

$$\text{CO}_{2,\text{corr}} = \text{CO}_{2,\text{amb}} - \left(\frac{\text{CO}_{2,\text{meas}}}{\text{NO}_{3,\text{meas}}} \right)_{\text{NO}_3\text{NO}_{3,\text{pure}}} \times \text{NO}_{3,\text{amb}} \quad (1)$$

The NO_3^+ signal during ambient measurements, $\text{NO}_{3,\text{amb}}$, is multiplied by the correction ratio $\left(\frac{\text{CO}_{2,\text{meas}}}{\text{NO}_{3,\text{meas}}} \right)_{\text{NO}_3\text{NO}_{3,\text{pure}}}$, which is the ratio of the measured CO_2^+ , $\text{CO}_{2,\text{meas}}$, to the measured NO_3^+ , $\text{NO}_{3,\text{meas}}$, during the nebulisation of pure NH_4NO_3 . This is then subtracted from the ambiently measured CO_2^+ signal, $\text{CO}_{2,\text{amb}}$. During these experiments, the surface ionisation effect was also found to interfere with the CO^+ signal. This has previously been observed in AMS measurements but studies have chosen not to correct for it because not enough measurements were gathered (Pieber et al., 2016). We therefore use the same relationship as Equation (1), with all CO_2 terms replaced with CO to find the corrected CO^+ signal. The correction ratio for CO^+ was higher (6.6%) than for CO_2^+ (3.5%), which shows the need to include this correction when fitting CO^+ independently.

2.3. Measurements of OC/EC, WSOC and elements

Organic carbon (OC) and elemental carbon (EC) concentrations were measured in triplicate for each filter sample ($\sim 0.54 \text{ cm}^2$ punches) using thermal optical carbon analysis (Model: DRI, 2001A). The IMPROVE-A protocol was followed which, in brief, ramps the temperature (140, 280, 480, 580, 740 and 840°C) in a helium and oxygen environment (Chow et al., 2004). This allows for the quantification of different fractions of OC (OC1, OC2, OC3 and OC4) and EC (EC1, EC2 and EC3), along with pyrolyzed carbon (OP). The OC/EC analyser was calibrated in 4.8% CO_2 and 95.2% helium. Peak area calibrations were performed daily using 5% CH_4 in 95% helium and an error of 3–7% was estimated for OC and EC concentrations.

Water-soluble organic carbon (WSOC) was measured using a total organic carbon (TOC) analyser (Shimadzu TOC-L CPH/CPN, Japan) and a catalytic combustion oxidation method. Punches ($\sim 0.4 \text{ cm}^2$) of each PM_{10} filter were extracted in ultrapure Milli-Q water (18.2 M $\Omega \text{ cm}$) and sonicated in triplicate for 45 min at 50°C . A platinum catalyst at 680°C was used to convert the carbon in filtered (0.2 μm pore) extracts (5–10 mL) into CO_2 which was measured by a nondispersive infrared detector (NDRI). Consecutively, inorganic carbon in the water extract was determined by measuring the evolved CO_2 from another sample aliquot after it was acidified (pH 2) with 25% phosphoric acid. The NDIR detector response for inorganic carbon was calibrated with a Na_2CO_3 standard. WSOC was estimated from the difference between the total carbon and the inorganic carbon. The water-insoluble organic carbon (WIOC) was then calculated by subtracting WSOC from the thermal optical carbon analyser OC measurement ($\text{WIOC} = \text{OC} - \text{WSOC}$). Standards of potassium hydrogen phthalate were used for calibration and blank filters were measured every 10 samples to correct for background concentrations. Triplicate sample analysis yielded a repeatability error of 3–10%.

A wavelength dispersive X-ray fluorescence spectrometer (WD-XRF, ZSX Primus, Rigaku, Japan) was used to measure the PM_{10} elemental concentrations of Al, B, Ca, Cl, Cr, Cu, Fe, K, Mg, Mn, Mo, Na, Ni, P, Pb, S, Ti, Zn and Zr. Measurements were taken under vacuum at 36°C and using a 2.4 kW tube rating. Micro-matter thin-film standards were used for calibration and samples were measured in triplicate with a repeatability error of 5–10%. Detailed information on the calibrations and measurements are described in previous publications for OC/EC, WSOC and WD-XRF measurements (Banoo et al., 2020; Jain et al., 2020; Sharma et al., 2014, 2021).

2.4. Meteorological measurements

Temperature and dewpoint temperature measurements are from Indira Gandhi International Airport in New Delhi at 1 h resolution (downloaded at: <https://ncdc.noaa.gov/>, last access: 03/02/2022). The relative humidity, RH , was calculated using the Magnus approximation:

$$RH = \exp \left(\frac{bc(Dp-T)}{(c+T)(c+Dp)} \right) \quad (2)$$

Here, Dp is the dewpoint temperature and T is the air temperature (in $^\circ\text{C}$), while b (17.625) and c (243.04°C), are constants which apply to the following set of atmospheric conditions: $0^\circ\text{C} < T < 60^\circ\text{C}$, $1\% < RH < 100\%$ and $0^\circ\text{C} < Dp < 50^\circ\text{C}$.

The planetary boundary layer (PBL) height and surface solar radiation downwards (SSRD) were taken from the ERA5 land model from the ECMWF (<https://cds.climate.copernicus.eu/cdsapp#!/home>) at 1 h and 0.25° resolution. Although Nakoudi et al. (2018) found the ERA5 model overestimated PBL height in Delhi during convective hours (9 a.m. - 12 p.m.), they reported a strong correlation between the SSRD and lidar measurements. For this study, only the relative change in PBL height between seasons is considered and the absolute values are not critical to the findings.

2.5. Source apportionment

Positive Matrix Factorisation (PMF) is a multivariate analysis tool commonly used to separate a data matrix of pollutant concentration time series into source “factors” (Paatero and Tapper, 1994). In this instance, we use the mass spectral profile of the organic aerosol (number of measured ions $m = 816$), m , of each filter sample ($n = 166$) and combine them to form a matrix, $m \times n$, with time series rows of m/z species, n . The model can be summarised as:

$$\mathbf{X} = \mathbf{F}\mathbf{G} + \mathbf{E} \quad (3)$$

where the measured $m \times n$ data matrix, \mathbf{X} , is equal to the factor profile $m \times p$ matrix, \mathbf{F} , multiplied by the factor time series $p \times n$ matrix, \mathbf{G} , plus, the residual $m \times n$ matrix, \mathbf{E} . The user determines the number of factors, p , using the value of Q which is calculated as follows:

$$Q = \sum_{i=1}^m \sum_{j=1}^n \left(\frac{e_{ij}}{\sigma_{ij}} \right)^2 \quad (4)$$

Here, e_{ij} and σ_{ij} are the residual and measurement matrices, respectively. A Q value of 1 equates to a model solution that perfectly describes the measured data with all measurement uncertainty incorporated within the residuals. Optimisation of Q is achieved by increasing p until the change in Q , ΔQ , is small, which signifies that an increase in factors no longer improves the solution. The PMF2 algorithm was used in robust-mode using the Multilinear Engine 2 (ME-2) (Paatero, 1999) to explore the a (anchor)-value space when anchor profiles are used. The PMF Evaluation Tool (PET, v3.00) was used for more general solution exploration as it requires less CPU and less time than ME-2 (Ulbrich et al., 2009). The error matrix was down-weighted based on the conditions set out by Paatero and Hopke (2003), i.e. species with a signal-to-noise ratio (SNR) < 2 are down-weighted by a factor of 2 and species with a SNR < 0.2 by a factor of 10.

The error matrix was composed of both the AMS measurement uncertainties, α_{ij} , and the combined background concentrations of the solvent and the wash cycle, β_{ij} . The error has been calculated this way in previous offline-AMS studies (Bozzetti et al., 2017; Daellenbach et al., 2016) and uses the following equation:

$$\sigma_{ij} = \sqrt{\alpha_{ij}^2 + \beta_{ij}^2} \quad (5)$$

where, α_{ij} , is calculated according to statistical counting errors and ion-

tion variability as described in Allan et al. (2003).

The PMF solution presented here was determined using analyses described in SI Section S4.

2.6. Calibration of offline analyses

The input matrices were converted to atmospheric concentrations using the OM/OC ratios measured by offline-AMS, $(\frac{OM}{OC})_{\text{offline-AMS}}$, and the OC measurements, $OC_{OC/EC}$, made by the thermal optical carbon analyser using the relationship:

$$OM_{\text{amb}} = \left(\frac{OM}{OC}\right)_{\text{offline-AMS}} \times OC_{OC/EC} \quad (6)$$

in which OM_{amb} is the atmospheric organic matter concentrations calculated in units of $\mu\text{g m}^{-3}$.

The final 9-factor solution was chosen from over ~100 possible solutions using FPEAK rotations to explore the rotational ambiguity and using initialisation SEEDs. These can be described as pseudorandom

starting points from which the PMF model starts its analysis. The stability of each solution was also explored using bootstrapping analysis (50 runs) and the final 9-factor solution was the most stable. ME-2 was also used to anchor each solution to the online- PM_{10} profiles in a previous AMS study conducted in Delhi (Cash et al., 2021). The most significant difference in the profiles of the PM_{10} filters when run unconstrained compared to the anchored solution was the level of oxidation in the POA factors. This caused unusual results that no longer resembled recognisable source factors. We therefore continued to use the unconstrained PMF model solutions and more details on the choice of the solution is given below.

3. Results

3.1. PMF factor identification

The factor profiles and concentration time series for the 9-factor solution are presented in Fig. 3, along with the time series of tracers to help identify each factor. There are two traffic-related factors, one

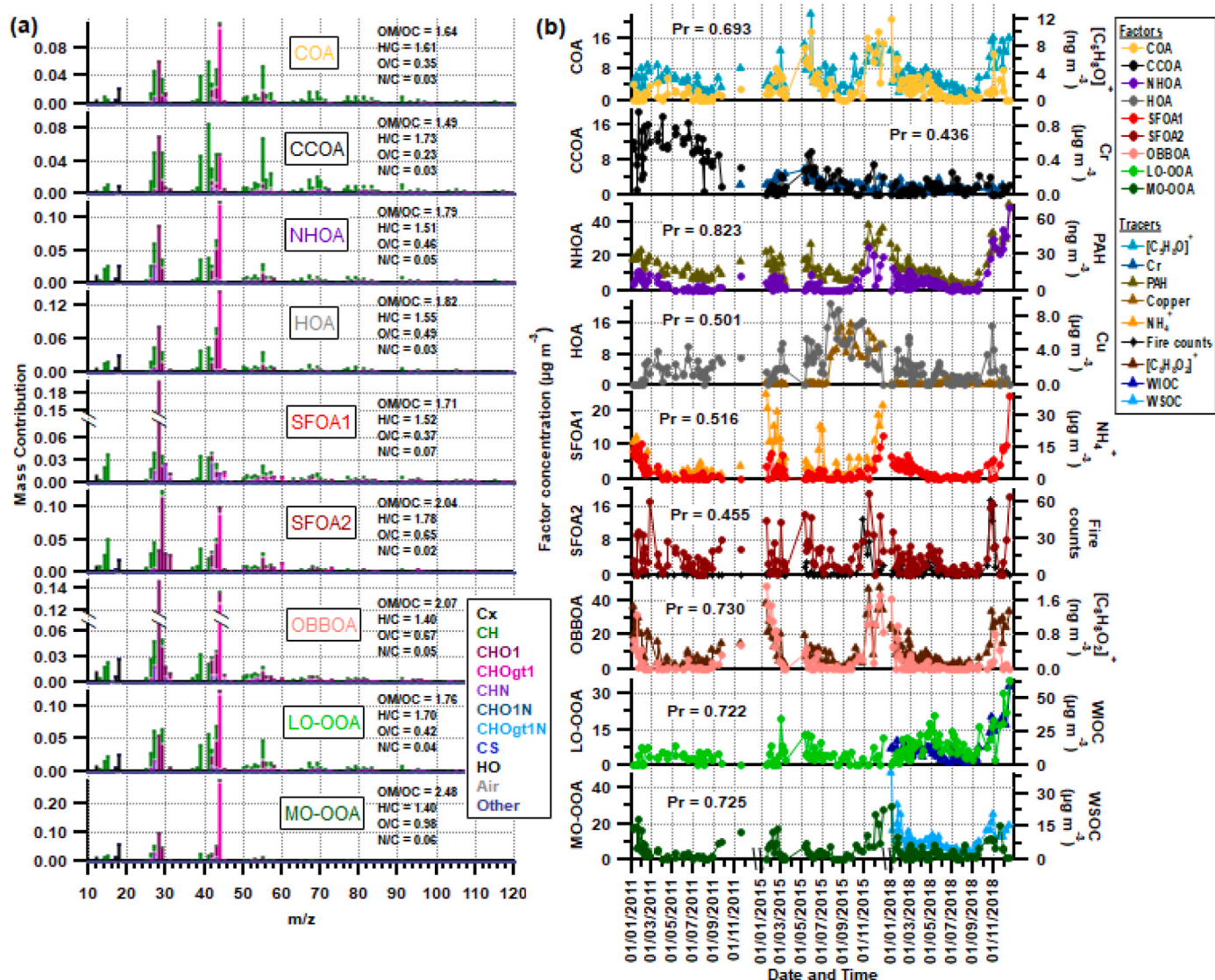


Fig. 3. (a) Factor profiles and (b) factor concentration time series for the 9-factor solution. The profiles for factors SFOA1 and OBBOA have split y-axes to display more detail of their composition. Elemental analysis ratios for OM:OC, H:C, O:C and N:C are shown for each factor in (a). The tracer time series (right y-axis) for each factor underlie each graph in (b) and the Pearson's r (Pr) correlations between factor and tracer are also shown. Note: for some tracer species, the measurements are not complete for all three years. The AMS measured ions, $[\text{C}_5\text{H}_8\text{O}]^+$ and $[\text{C}_8\text{H}_8\text{O}_2]^+$, respectively represent a tracer used to identify cooking OA and a fragment of dibenzodioxin called benzodioxan.

named hydrocarbon-like organic aerosol (HOA) and the other named nitrogen-rich HOA (NHOA), and three burning-related factors, two of which are linked to different sources of solid-fuel burning (SFOA1 and SFOA2), while another is linked to aged and more oxidised biomass burning OA (OBBOA). There is also a factor relating to coal-combustion OA (CCOA), another to cooking OA (COA), and two secondary OA factors separated based on their oxygen content: less-oxidised oxygenated OA (LO-OOA) and more-oxidised OOA (MO-OOA). The attribution to sources and naming is based on the comparison of mass spectra with those identified in previous studies, including the presence of individual characteristics such as a higher m/z 55 to m/z 57 ratio for COA than for HOA (Mohr et al., 2012) and the presence of m/z 60 and m/z 73 (levoglucosan) in factors containing biomass burning emissions (see below). Encouragingly, the PMF analysis did not identify a factor that reflected the solvent itself providing further evidence that the scrubbers were efficient in removing the acetone.

The traffic factor, HOA, has the strongest correlation of all factors with Cu (Fig. 3) which is a well-known tracer for traffic-related (non-exhaust emission) PM_{10} due to the wear of metallic brake pads on vehicles (Denier van der Gon et al., 2007; Harrison et al., 2021). The second traffic factor, NHOA, has a similar mass profile and elemental composition to HOA, except NHOA has higher nitrogen-containing family peaks (CHN and CHO1N) and a higher N:C ratio (Fig. 3). The NHOA factor has previously been observed in Delhi using online-AMS measurements and a similar distinction was made where one traffic

factor is richer in nitrogen (Cash et al., 2021). Another study also observed a separation of traffic-related volatile organic compounds (VOCs) into two PMF factors (Wang et al., 2020). These studies have made the link between the second (NHOA) traffic factor and heavy goods vehicle (HGV) restrictions occurring during the day. These restrictions cause a large influx of mostly diesel-engine HGVs into the city during the evenings and early hours of the morning.

The NHOA factor shows a strong correlation with PAHs (Pearson's $r = 0.823$) and since diesel engines emit large concentrations of PM PAHs (Singh et al., 2020) this supports diesel emissions contributing to NHOA. Through offline-AMS measurements, a total of 15 PAHs were measured on the filters which are mostly unsubstituted PAH species; all have been measured in previous AMS studies (Herring et al., 2015). The profiles of these PAH species in each factor are shown in Fig. 4. The breakdown of total PAH mass into factors is also shown, along with the percentage composition of PAHs within each factor. Fig. 4 shows NHOA has the highest composition of PAHs (0.733%) and contributes the largest proportion to total PAH mass (21.5%). There is some indication that the NHOA factor PM concentrations have increased over the years (Fig. 3).

The factor mass profile of nitrogen species is also shown in Fig. 4. The high N:C ratio of NHOA is mostly due to the m/z 27 peak. This relates to the ion $[CHN]^+$, which is a fragment of multiple possible nitrogen-containing species. Previously, NHOA has been shown to be composed of nitrile species (Cash et al., 2021) but this is not evident in the spectrum in Fig. 4. This suggests some of the nitrogen containing species

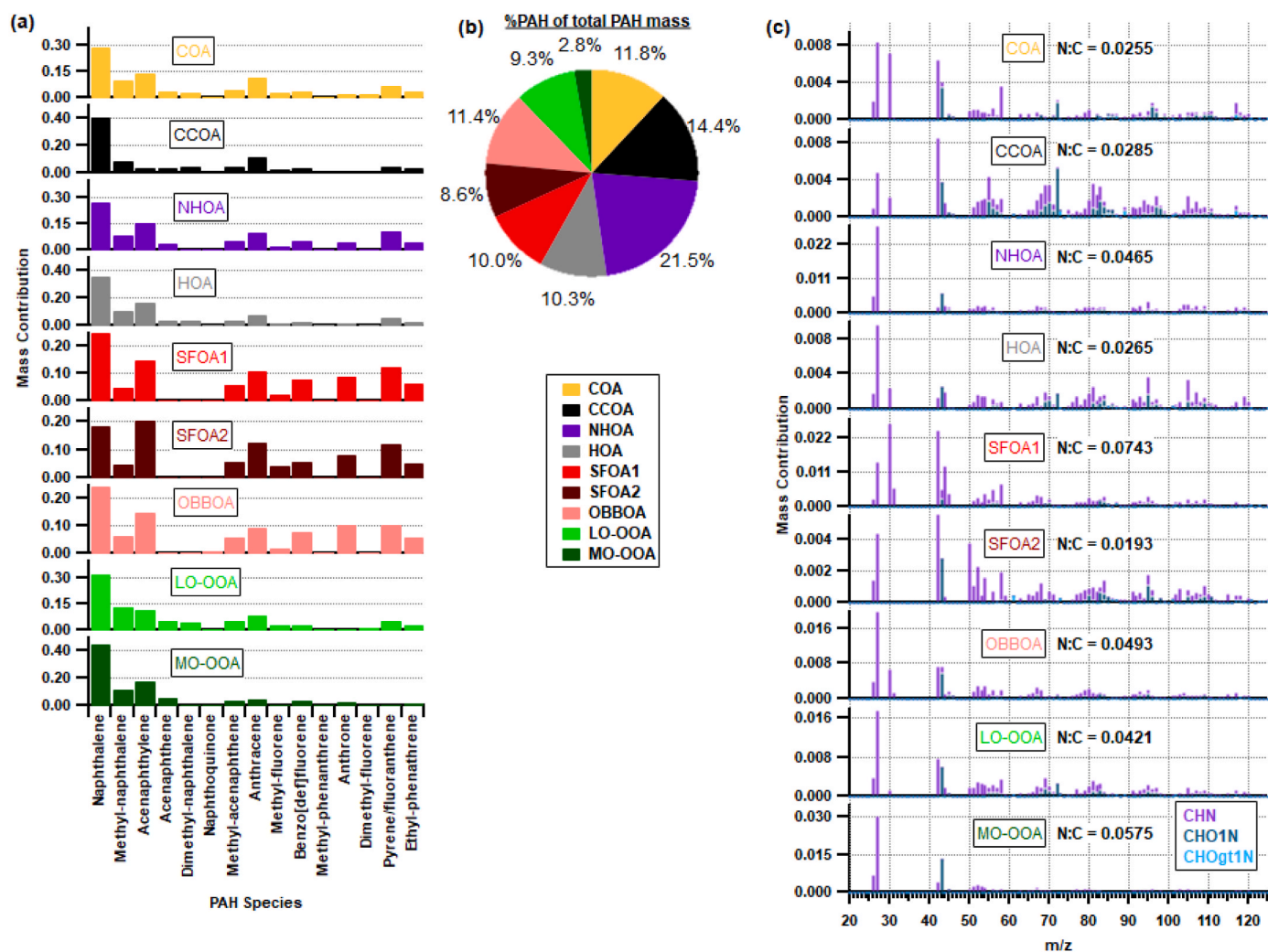


Fig. 4. Factor profiles for (a) polyaromatic hydrocarbons (PAH) and (c) nitrogen species. The pie chart (b) shows the percentage contribution of factors to the total PAH mass.

have not been extracted or have volatilized from the filter sample, highlighting a limitation of the offline-AMS technique.

The COA factor has a particularly high m/z 55:57 ratio and has a strong correlation with the AMS-measured cooking tracer ion, $[C_5H_8O]^+$ (Fig. 3). These two characteristics are indicators of cooking OA (Sun et al., 2016). Previous PM_{10} measurements in Delhi suggest COA is highly oxygenated compared with this type of OA in other cities, presumed to reflect different cuisines (Cash et al., 2021). This is supported by the measurements from the current offline study as the COA profile has large m/z 28 and 44 peaks. These peaks also make the COA profile look particularly similar to the PM_{10} COA profile. It also has a similar set of H:C, O:C and OM:OC ratios. These similarities imply the majority of the PM_{10} COA mass is within the PM_{10} fraction.

The coal-combustion factor CCOA can be difficult to separate from other fossil fuel emission products such as HOA. However, the CCOA profile in this study has a ratio of C_xH_y peaks similar to that measured in previous AMS studies (Lin et al., 2019; Xu et al., 2016) (Fig. 5). Of the

available auxiliary measurements, it is expected that CCOA should correlate with Cu and Cr as these are bonded to the organic fraction of coal and are present in coal ash (Li et al., 2020; Pacyna et al., 2007; Reizer and Juda-Rezler, 2016; Tang et al., 2022). The correlation matrix of PMF factors with external tracers (Fig. 5) shows a moderate correlation of CCOA with Cr and a low correlation with Cu. However, in an urban setting, Cu may be dominated by other sources, such as traffic. Species often bonded to the mineral part of coal include As, Cd, Pb and Zn (Reizer and Juda-Rezler, 2016). These have moderate correlations with Cr which strengthens the suggestion that the moderate correlation between CCOA and Cr is another indicator that CCOA represents coal-combustion. The correlation between Cr and CCOA could also suggest that CCOA is influenced by coal-combustion from the metallurgy industry as chromium has been linked to the metallurgy industry in Delhi, and in other cities (Gao et al., 2019; Khillare et al., 2004; Kothai et al., 2008).

The three burning-related factors of SFOA1, SFOA2 and OBBOA

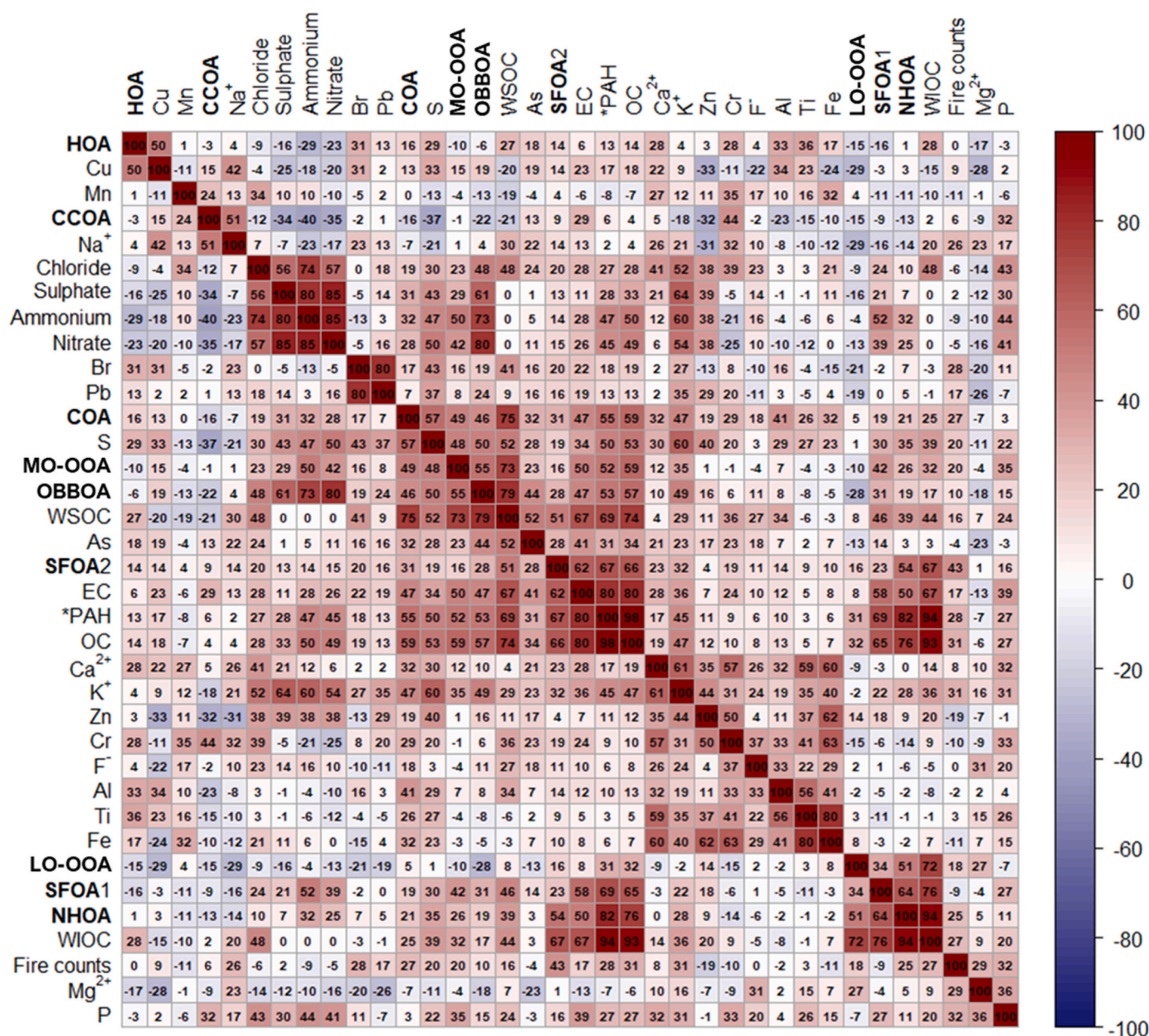


Fig. 5. Pearson's r correlation matrix between factors and external tracers ordered according to a hierarchical cluster analysis. *The PAH time series is internally measured by the AMS and is the sum of the species described in Fig. 4.

represent three different fuel-types as determined from their composition and through external tracers. SFOA1 has the characteristic levoglucosan m/z 60 and 73 peaks associated with wood burning (Fig. 3). It also has the second highest correlation, behind OBBOA, with NH_4^+ (Pearson's $r = 0.516$, Fig. 5), along with the highest nitrogen content out of all factors ($\text{N:C} = 0.0743$). From Fig. 4, the SFOA1 mass profile for nitrogen species shows large peaks at m/z 30 ($[\text{C}_4\text{HN}]^+$), m/z 42 ($[\text{C}_2\text{H}_4\text{N}]^+$), m/z 44 ($[\text{C}_2\text{H}_6\text{N}]^+$), m/z 56 ($[\text{C}_3\text{H}_6\text{N}]^+$) and m/z 58 ($[\text{C}_3\text{H}_8\text{N}]^+$). These peaks have been shown to derive from amine compounds in both AMS studies (Bottenus et al., 2018; Docherty et al., 2011) and other MS-based studies (Gohlke and McLafferty, 1962; McLafferty and Turecek, 1993).

The high nitrogen content of SFOA1 suggests it originates from the burning of nitrogen-rich fuels. Numerous studies have compared the PM burning emissions from commonly used solid fuels in Delhi (Jayarathne et al., 2017; Keene et al., 2006; Pervez et al., 2019) and have found that fuels rich in nitrogen, such as dung-cakes, emit large concentrations of ammonium. SFOA1 is therefore likely related to residents burning solid fuels to keep warm during the colder months. This is supported by a general increase of SFOA1 during the post-monsoon and winter seasons, whilst during the summer and monsoon seasons it is close to zero (Fig. 3).

The second solid-fuel factor, SFOA2, appears to be a mix of sources. Its mass profile has a particularly large peak at m/z 29 ($[\text{CHO}]^+$) when compared to OBBOA and SFOA1, highlighting a significant difference in its oxygenated composition. Its large m/z 60 and 73 peaks suggest it is

heavily influenced by wood or cellulose-based material burning, but it also has the highest composition of tracer peaks for municipal waste burning such as 1,2- or 1,4-dioxin (m/z 84, $[\text{C}_4\text{H}_4\text{O}_2]^+$), furan (m/z 68, $[\text{C}_4\text{H}_4\text{O}]^+$), phenol (m/z 94, $[\text{C}_6\text{H}_6\text{O}]^+$) and furfural (m/z 96, $[\text{C}_5\text{H}_4\text{O}_2]^+$) (Cash et al., 2021; Stewart et al., 2021). It also has the highest correlation of all factors with fire counts (Pearson's $r = 0.455$). The fire counts are from satellite measurements using the NASA Moderate Resolution Imaging Spectroradiometer (MODIS) sensor (for 2011) and the Visible Infrared Imaging Radiometer Suite (VIIRS) sensor (for 2015 and 2018) (available at: <https://earthdata.nasa.gov/earth-observation-data/near-real-time/firms>, last access: 18 Jan 2022). The fire counts were limited to a custom polygon encompassing the Haryana region. The vast majority of the fires counted within this region were during April–May and October–November. This identifies the fires as originating from the burning of crop-residue from the wheat and rice harvests.

The third burning-related factor, OBBOA, has moderately large levoglucosan tracer peaks (m/z 60 and 73). It also has a low H:C ratio and a high O:C ratio (Fig. 3) which indicates it is highly oxidised and therefore more secondary in its composition. This suggests OBBOA is from a mixture of local sources, city-wide sources, and sources along the Indo-Gangetic plain, as predicted by back-trajectory studies using the same PM_{10} filters (Banoo et al., 2020).

The highest contributions to OBBOA concentrations arrive via a westerly wind, which is the same for both SFOA1 and SFOA2 (Fig. 6). The OBBOA factor may therefore represent an aged and oxidised

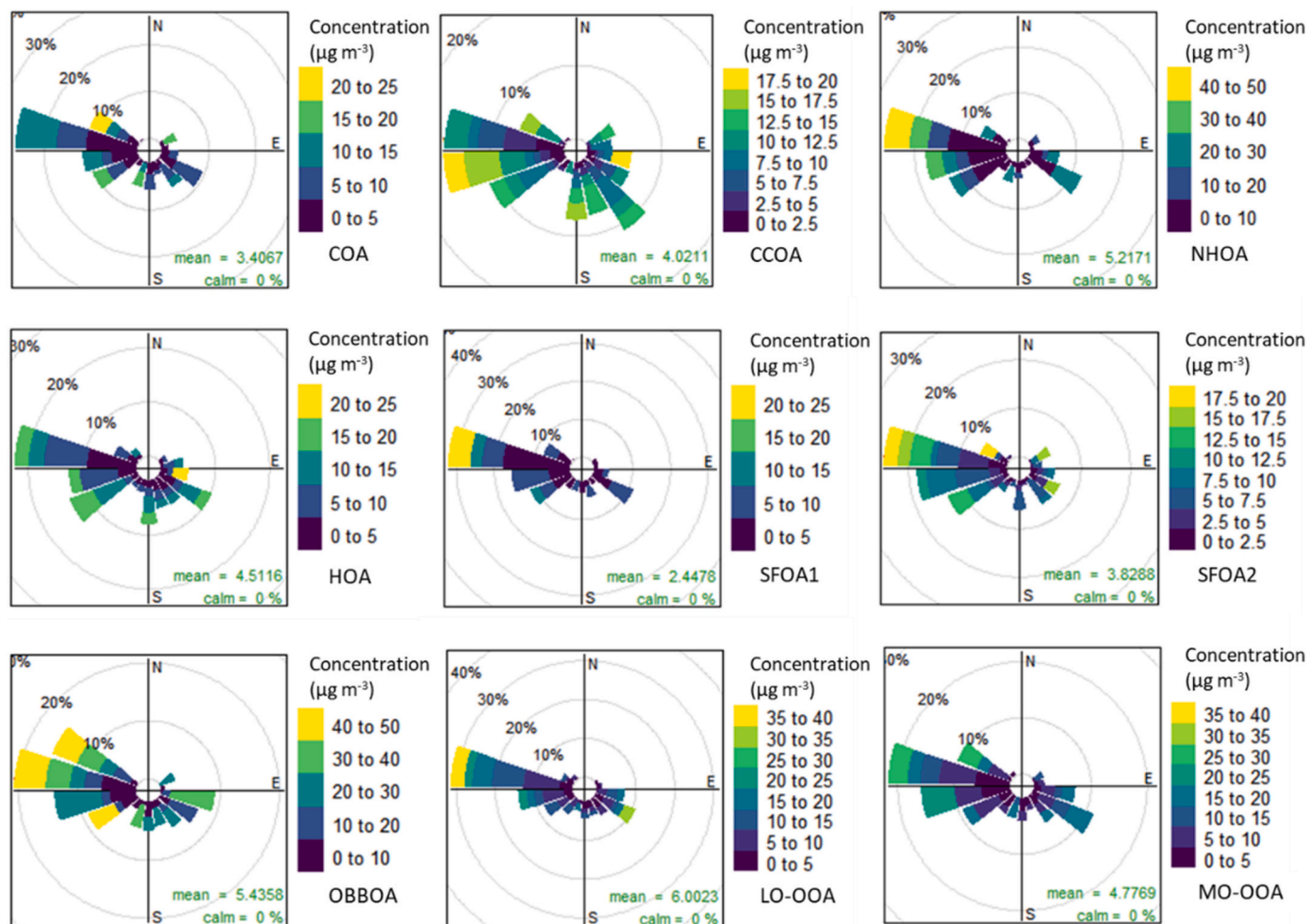


Fig. 6. Pollution roses for each factor showing wind vectors sized to represent the percentage contribution to the mean concentration. The wind vectors are divided into the concentration bins described in each legend.

mixture of SFOA1 and SFOA2. This is supported by the high N:C ratio (0.0493) which coincides with N-rich SFOA1. It also has a high correlation with benzodioxan (Pearson's $r = 0.730$, Fig. 5) which is an AMS-measured fragment species of polychlorinated dibenzodioxins (PCDDs). PCDDs have previously been suggested to originate from municipal waste burning (Cash et al., 2021) and to be a significant source of chloride PM in Delhi. This is supported by OBBOA having the highest correlation of all the factors with chloride (Pearson's $r = 0.480$).

The two oxygenated OA factors, LO-OOA and MO-OOA, have similar profiles but they characteristically differ in their oxygenation as shown by their O:C ratio (Fig. 3). The large O:C ratio of MO-OOA is mostly driven by the large m/z 44 peak, $[\text{CO}_2]^+$, which is often thought of as a fragment of acidic functional groups (Duplissy et al., 2011). This means MO-OOA is highly water-soluble and, as expected, has a strong correlation with WSOC measurements (Pearson's $r = 0.725$). Similarly, the higher H:C, and lower O:C, of LO-OOA means it is less water-soluble, and it is strongly correlated with water-insoluble organic carbon measurements (WIOC) (Pearson's $r = 0.722$). This supports the findings of high recoveries of water-insoluble OA when using this offline-AMS method.

4. Discussion

4.1. Seasonal and annual comparisons of PM₁₀ across 2011, 2015 and 2018

The seasonal average concentrations of the 9 PMF factors across the four seasons in each year are shown in Fig. 7. The highest concentrations of PM₁₀ OA for the winter, pre-monsoon and monsoon seasons occurred in 2015. However, the post-monsoon concentrations were comparably high in 2015 and 2018. The post-monsoon of 2018 was meteorologically different to both 2011 and 2015. The temperatures in 2018 were slightly lower and the relative humidity was slightly higher (Fig. 2). The average planetary boundary layer height (PBL) was also lower during the mornings of the 2018 post-monsoon, as shown by Fig. 8. Therefore, the lower PBL may have accentuated the PM₁₀ concentrations.

Fig. 7 shows that traffic (=NHOA+HOA) is a consistently large contributor to PM₁₀ OA in all three years. The consistency of traffic concentrations is mostly due to HOA because NHOA is less consistent

across all seasons. NHOA is particularly low in concentration during the monsoon period, suggesting a greater susceptibility to atmospheric washout. However, peak concentrations occur during the post-monsoon which is mostly due to an increase in NHOA.

The rapid increases in population and vehicles from 2011 to 2018 might suggest that traffic concentrations should also increase across the years. That this is not reflected in the traffic PM₁₀ OA annual averages is likely because of the implementation of the Bharat stage (Table 1) tailpipe emissions standards. There is also a decrease in traffic concentrations from 2015 to 2018 during the pre-monsoon which is the season least affected by a low boundary layer (Fig. 8).

COA has a large presence during most seasons which is expected as cooking is a daily activity. However, there is a drop in concentrations during the monsoon period, which is likely due to increased rainfall events causing food vendors and customers to stay inside, as well as to washout (Fig. 7).

CCOA is consistently the largest individual OA factor across the three seasons of winter, summer and monsoon during 2011 (Fig. 7), showing that coal-combustion was a significant source of OA in 2011. CCOA concentrations then start to decline in 2015 which is expected as the use of coal has decreased in popularity commercially, in homes and, in particular, for thermal power stations. During 2018, CCOA concentrations decrease further and are almost at zero in October. This coincides with the eventual shutdown of the Badapur thermal power station (~20 km southeast of the measurement site) in October 2018, following the shutdown of the Rajghat power station in October 2015.

The three burning-related factors of SFOA1, SFOA2 and OBBOA can be combined to represent the source category of burning-related OA. From Fig. 7, burning-related OA was the largest contributing source during the winter. It was also the largest OA source during the post-monsoon of 2011 and 2015. This makes burning OA the most significant source when concentrations of PM₁₀ are at their highest. This has been observed previously in the PM₁ OA measurements in Delhi where burning-related PM source factors were the highest during the post-monsoon (Cash et al., 2021). However, it is important to note that burning-related emissions appear to be on the decline, as the highest mass of burning-related OA is in 2015 (Fig. 7). The concentrations then decrease in 2018 which suggests that peak emissions of burning-related

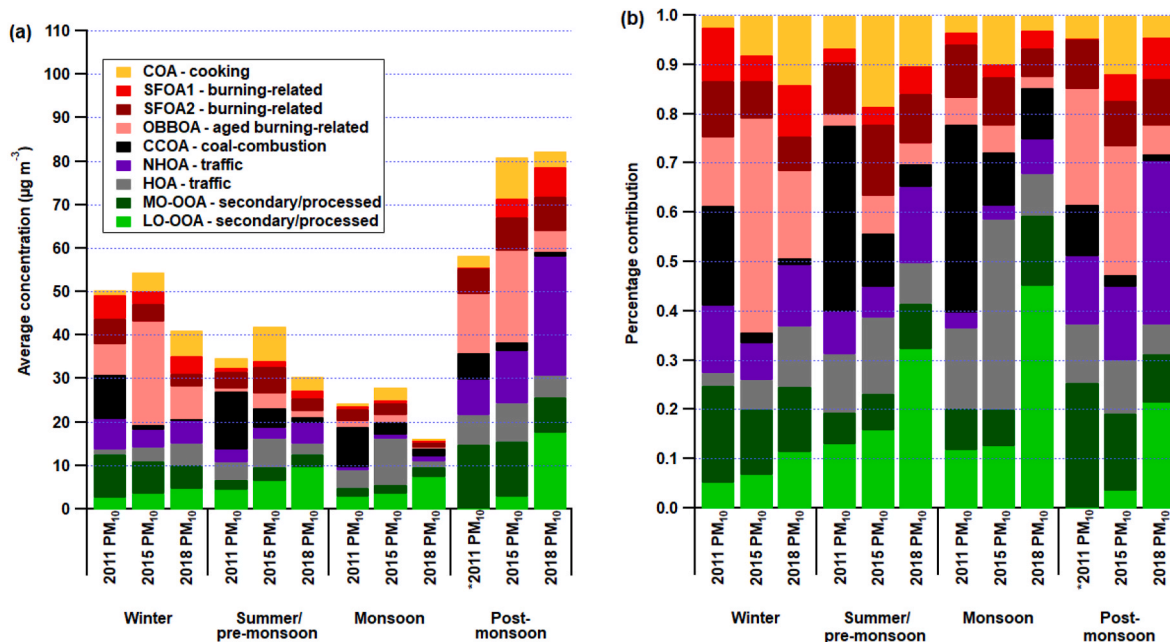


Fig. 7. Average concentrations of PM₁₀ OA factors (a) and percentage contributions of factors to total PM₁₀ OA (b) during each of the four seasons of the years 2011, 2015 and 2018. *The PM₁₀ concentrations for factors during the post-monsoon of 2011 are from one filter sample only due to the unavailability of filters during this period.

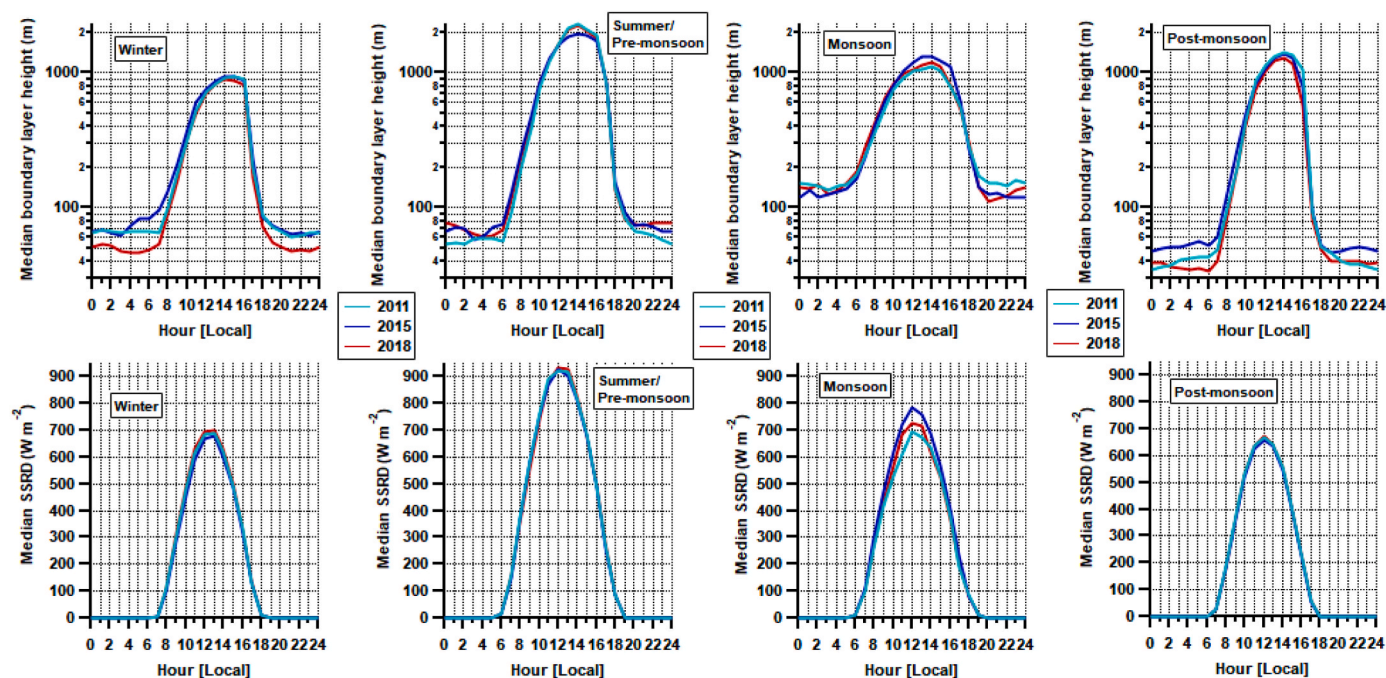


Fig. 8. Median diurnal cycles of planetary boundary layer height (PBL, first row of graphs) and surface solar radiation downwards (SSRD, second row of graphs) for each of the four seasons and for each of the years 2011 (cyan), 2015 (blue) and 2018 (red). The y-axis in graphs displaying PBL are logarithmic in order to show the daily minimum more clearly. Values shown are the average across the entire season.

PM may have been reached.

Differences in the seasonal averages of individual burning-related OA factors are apparent (Fig. 7). As discussed, SFOA1 is shown to be linked to wood and dung-cake burning by residents keeping warm during the colder months. This is reflected in the increase in SFOA1 average concentrations in the winter and post-monsoon seasons. For SFOA2, peak concentrations are observed in the post-monsoon season. This is most likely due to its links to crop-residue burning which, from fire-count observations, occurs most frequently during October, consistent with the burning of the kharif season rice residue (Montes et al., 2022).

The seasonal trends in LO-OOA and MO-OOA suggest different sources influence their formation. The concentrations of MO-OOA are generally larger than LO-OOA during the winter and post-monsoon (Fig. 7) but MO-OOA is smaller than LO-OOA during the pre-monsoon and monsoon. The burning-related OA sources (SFOA1, SFOA2 and OBBOA) show a similar pattern to MO-OOA, i.e. they are also lower in concentration during the pre-monsoon and monsoon periods. Therefore, MO-OOA most likely has a significant contribution from the oxidation of burning-related emissions. Conversely, LO-OOA increases in concentration during the pre-monsoon and monsoon periods. Fig. 8 shows that the maximum diurnal solar radiation is greatest in the pre-monsoon and monsoon seasons, as expected given these seasons span the summer solstice. This suggests LO-OOA partially derives from photooxidation of VOCs.

The MO-OOA factor shows a gradual decrease in concentration each year (Fig. 7) which suggests that, in general, the impact of burning-related PM in Delhi has been diminishing. The opposite trend is apparent for LO-OOA, which shows a gradual increase in concentration each year. The increase is not likely to be due to meteorology because solar radiation (i.e. the meteorological control of LO-OOA) shows minimal change between each year (Fig. 2). This suggests that sources of PM affect its formation as well. NHOA also shows a gradual increase each year (Fig. 7). During 2018, there is a particularly large peak in concentrations during the post-monsoon, which is also reflected in the concentrations of LO-OOA. This is supported by a relatively strong correlation between NHOA and LO-OOA (Pearson's $r = 0.510$, Fig. 5).

LO-OOA may therefore be influenced by diesel emissions and the annual averages in Fig. 7 suggest LO-OOA could continue to increase in the future without more diesel-focused emission mitigation strategies.

4.2. The recovery of primary organic aerosol factors using the developed offline-AMS method

Overall, the results in Fig. 7 show the dominant contributors to OA are primary (POA) factors. As previously discussed, OA recoveries for individual PMF factors are not currently determined for the offline-AMS method used in this study; consequently, the results represent OA that is soluble in 1:1 acetone-water solvent. However, the POA factors that are particularly insoluble in water (e.g. HOA and COA) are dominant in the total OA mass measured. This shows that POA factors can be extracted with high recoveries with our offline-AMS method.

Our previous online-AMS PM₁ measurements in Delhi from 2018 (Cash et al., 2021) confirm a number of important aspects of the offline-AMS method developed in this work. Firstly, the offline-AMS method has retained compositional details such as the high PAH content in factors COA, HOA, NHOA and SFOA. The method also retains important tracer ions, even those that are particularly low in concentration such as the benzodioxan ion which relates to PCDDs. Secondly, despite the lower temporal resolution of the filters analysed by offline-AMS, there is a separation of traffic-related PM into two factors, one of which contains a greater N:C ratio (NHOA). Thirdly, the offline-AMS method has delivered similar factor seasonal averages, particularly for the pre-monsoon and monsoon seasons. All the above indicate that the offline-AMS method has successfully captured the majority of the OA in Delhi's atmosphere. Future work aimed at determining PMF factor recoveries when using 1:1 acetone-water solvent would be beneficial. The offline analysis presented here identified two factors that were not isolated in the online dataset: the first is CCOA, which is consistent with the decline of this component over the years to very small concentrations by 2018. The other is a difference in the split of SFOA into two factors in the offline analysis, distinguishing between biofuels (e.g. dung cakes) and other burning. This may reflect the fact that the solution of the offline analysis is defined also by changes from

year to year, whilst the solution of the online data is driven also by diurnal variability.

However, some limitations to the developed offline-AMS method have been highlighted. One of these is the lack of nitrogen species in the NHOA mass profile. The quantification and detection of nitrogen species using HR-TOF-AMS is often considered uncertain, although some studies have shown it is possible (Bottenus et al., 2018; Docherty et al., 2011). This is because nitrogen-containing species are often situated on the tail-end of large neighbouring peaks in the mass spectrum. Therefore, there is already uncertainty involved with measuring N-containing species. However, it is also likely the offline-AMS method does not recover some N-containing species.

There is also a lack of oxygen-containing PAHs in the offline-AMS profiles, which were previously shown to be key peaks in the mass spectra of some PMF factors (Cash et al., 2021). This suggests that some complex and highly insoluble species are not recovered by the offline-AMS method.

4.3. The presence of open waste burning

In 2015 and 2016, there were complete bans on open waste and crop-residue burning (Table 1), but to what extent these bans have been enforced effectively is uncertain when reviewing literature (Gulia et al., 2018). The general decrease in burning-related OA from 2015 to 2018 could suggest that the bans are having an effect. However, the composition of both SFOA2 and OBBOA show a substantial amount of their mass originates from municipal waste burning. This suggests that open burning still occurs and it is clear that further mitigation strategies are needed to reduce municipal waste burning PM more effectively, as well as burning as part of industrial processes such as the processing of electronic waste.

4.4. The decline in coal combustion

In order to meet the electricity demands of the second largest population in the world, India has a large number of coal-fired power stations and a significant percentage of its electricity is generated from these stations (~60%) (Yang and Urpelainen, 2019). Two coal-fired power stations are situated within the national capital territory (NCT) of Delhi: the Rajghat thermal power station (~8 km east) and the Badarpur thermal power station (~20 km southeast) (Suneja et al., 2020).

As discussed above, the CCOA factor shows a decline in concentrations across the three years (Fig. 3). This coincides with the gradual decrease in popularity of coal as a fuel due to public knowledge of air quality issues and government decisions to shut down power stations. This can be seen more clearly in the annual wind directional data in Fig. 9. There is a larger spread of peaks in concentration during 2011 when compared to 2015 and 2018, suggesting a greater number of sources of CCOA were active during 2011. The high peaks in concentrations during 2011 originate from the direction of the two thermal power stations (east and southeast). There are also high concentrations

in south and south westerly winds. This implicates the large industrial areas (~5 km, Mayapuri industrial areas named “phase 1” and “phase 2”) in this direction which likely relied on coal combustion for power or industrial use. High concentrations also originate from the west and northwest which is mostly residential areas and small businesses (~3 km, Kirti Nagar). In these areas coal is used as a fuel for cooking and heating which shows contributions of domestic coal combustion. Domestic coal combustion from cooking using tandoor stoves has previously been shown to be a moderate contributor to PM_{2.5} (Gulia et al., 2018). Modelling of PM_{2.5} emissions sources shows that a ban on coal-fired tandoors in hotels and restaurants could reduce PM_{2.5} concentrations by up to 9% (Gulia et al., 2018).

Moving from 2011 to 2015, the contributions of CCOA from the east began to lessen in 2015 and this could mark the gradual decline in use of the Rajghat thermal power station which was eventually shut down in October 2015. The contributions from the west are still the largest but this also decreases in intensity which suggests the domestic use of coal has declined. This coincides with the predicted increase in popularity of electricity, liquid petroleum gas or natural gas being used for heating and cooking in residential homes and small businesses (Negi and Kumar, 2019). There are still large peaks in concentration from the southwest. This suggests that the industrial use of coal is still a high contributor to CCOA in 2015. Although only small contributions are seen from the southeast, it is likely that the Badarpur thermal power station still contributes a significant amount to areas of Delhi.

A similar trend is apparent comparing 2015 with 2018, as there is a decrease in the contribution of CCOA from all wind sectors. There are still contributions of CCOA originating from the southeast; however, the shutdown of the Badarpur thermal power station in October 2018 likely means CCOA emissions from this wind sector will be minimal in future years. The west is the largest contributing wind sector for 2018 which suggests coal combustion still occurs in households and small businesses.

Based on this wind sector analysis it is therefore likely that the two power stations had a large influence over CCOA concentrations, particularly during 2011. Combined with the general decrease in use of coal in industry, small businesses, and residential homes, this has caused a significant decrease in CCOA. Using the annual averages from 2018 to 2011, there is an 87% decrease in CCOA which results in a predicted 17% decrease in total PM₁₀ OA. The decision to shut down the two thermal power stations has therefore been a successful air quality mitigation strategy that effectively reduced the concentrations of PM₁₀ from coal-combustion. It is likely that concentrations of CCOA are, however, higher in residential and industrial areas as coal-combustion is still ongoing in homes and businesses. Further reductions could therefore be realised via the widespread use of electrical appliances for cooking and other non-emitting methods of generating electricity for industry.

The Indian government have recently implemented periodic bans on coal and wood burning for cooking food in restaurants and eateries (Goyal et al., 2019; Jonidi Jafari et al., 2021). It would be helpful for future studies to investigate the change in PM₁₀ due to these measures.

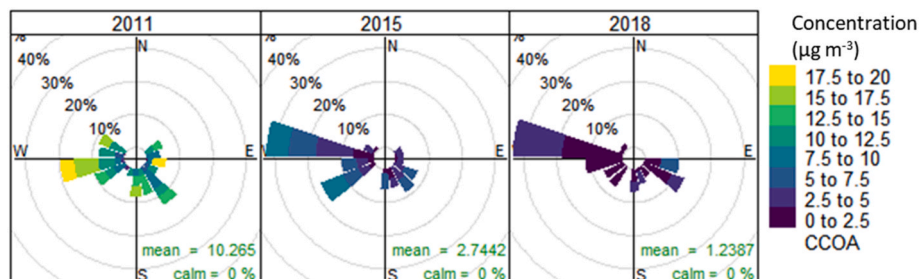


Fig. 9. Pollution roses for coal-combustion organic aerosol (CCOA) in 2011, 2015 and 2018. The wind vectors are sized to represent the percentage contribution to the mean concentration and divided into the concentration bins described in the legend.

4.5. The increase in diesel-related PM concentrations and the efficacy of HGV restrictions

Diesel emissions have previously been compared to CNG and petrol emissions, and are shown to be the largest contributor to PM concentrations in Delhi (Goel and Guttikunda, 2015; Singh et al., 2020). The majority of the traffic PM tailpipe emissions originate from diesel-engine HGVs, despite them being lower in numbers compared to cars, two-wheelers and three-wheelers (Singh et al., 2018). There is also a moderate contribution from diesel-generator sets which are used by homes and businesses when there are electricity power cuts (Gulia et al., 2018). These events tend to be more common in pre-monsoon and monsoon seasons when electricity supplies come under pressure from air conditioning and heavy rain events.

As discussed, the composition of NHOA suggests it is related to diesel-engine emissions. The NHOA concentrations are particularly low during the monsoon which could be due to washout, however, NHOA concentrations are larger than HOA during the post-monsoon and winter. This could be explained by HGV restrictions (7:00 a.m. to 10:00 p.m.) occurring when there is a low PBL height during the winter and post-monsoon (Fig. 8), thereby amplifying the concentrations. This phenomenon was observed in 2018 when PM₁ concentrations in Delhi were strongly influenced by the low PBL height (Cash et al., 2021). The same study showed strong peaks in the diurnal concentrations of NHOA during the late evening and early morning (Cash et al., 2021). The PBL height was also lower during the 2018 post-monsoon compared to 2011 and 2015 (Fig. 8). This likely further accentuated the concentrations and, as a result, NHOA concentrations are particularly high during this period (Fig. 7).

Therefore, despite the restrictions already in place, there appears to be scope to reduce Delhi's PM concentrations by further targeting diesel emissions. Current regulations permit HGVs, the highest emitting vehicle type, to enter the city at a time with unfavourable meteorology. Therefore, if the priority of the HGV restrictions is to reduce PM concentrations (but possibly not exposure), it is likely beneficial to change the restrictions to allow HGVs to enter during the middle of the day, when the PBL is high. However, this does not consider traffic congestion. It would therefore be beneficial for future studies to focus on the change in PM concentrations when HGVs enter the city during the middle of the day, while incorporating the effects of PBL height and traffic flow and people movement.

5. Conclusions

This study used an offline-AMS method to analyse filter samples collected over the years of 2011, 2015 and 2018 at the CSIR-National Physical Laboratory in Delhi to assess temporal changes in source contributions to Delhi's organic aerosol (OA) and thus to particulate matter (PM) in general. A high-throughput offline-AMS method was developed that could extract a high proportion of the primary organic aerosol (POA) fraction from PM filter archives. This was achieved using a solvent mix of 1:1 acetone to water for extraction. The method gave minimal organic background concentrations (~1% of the measured signal), and high recoveries of total OA ($95.4 \pm 8.3\%$).

Source apportionment analysis was performed on the organic fraction using Positive Matrix Factorisation (PMF). A total of nine factors were resolved which can be grouped into four primary source categories of OA: cooking, traffic, coal-combustion and other burning-related (solid fuel or open waste burning), as well as secondary OA contributions from regional burning and other sources. These results were compared with online-AMS measurements taken during the post-monsoon of 2018 at another location in Delhi. The majority of the compositional traits of PMF factors were resolved in the offline-AMS measurements, for example municipal waste burning tracers and polyaromatic hydrocarbon (PAH) content. The seasonal averages of factors derived from the filter archive also show similar trends despite different measurement

sites being used. Although the offline-AMS results show the evolution of PMF sources across multiple years in Delhi, it must be noted that filters from only three years were analysed. Future work is also required to estimate factor-specific OA recoveries to fully quantify PMF source factors. However, as overall OA recovery is high in this study, it is unlikely that the absence of factor recoveries will introduce major uncertainty in the measurement.

Annual PM₁₀ OA concentrations were the highest during the winter, pre-monsoon and monsoon of 2015, however, peak concentrations were measured during the post-monsoon of 2018. The seasonal analysis of total OA shows average concentrations decreasing in the order post-monsoon, winter, pre-monsoon, monsoon.

Burning sources were the largest contributor to OA during the winter and post-monsoon when PM₁₀ concentrations were at their highest. In 2018, there was also a 47% decrease in burning related OA concentrations which may indicate that peak concentrations were reached in 2015. This could, in part, be due to the 2015 ban on open waste burning and the 2016 ban on crop-residue burning, suggesting these mitigation strategies have had beneficial effect on PM₁₀ concentrations. However, compositional analysis of burning-related factors implies a substantial contribution from municipal waste burning which provides evidence that open waste burning is still occurring. This suggests that additional mitigation strategies have the potential to reduce burning-related PM concentrations further, such as improved municipal waste collection and more control over small industrial processes.

A gradual decline in annual OA measurements from coal-combustion sources is coincident with the shutdown of the Rajghat thermal power station in 2015 and the Badarpur thermal power station in 2018. This mitigation strategy, combined with initiatives to decrease the popularity of coal use in businesses, industry, and residential homes, have been effective in reducing OA from coal-combustion sources by 87%, corresponding to a 17% decrease in total PM₁₀ OA.

The rapid increase in Delhi's population and registered vehicles coincides with only moderate increases in traffic-related OA concentrations. This is most likely due to the introduction of tailpipe emission standards. This suggests the introduction of successively more stringent Bharat stage emissions standards has helped to largely counter-balance the increase in vehicle numbers in the control of PM₁₀ concentrations.

There was a strong increase in OA originating from diesel emissions during the winter and post-monsoon periods over the period 2011 to 2018. This may be a side-effect of an air pollution mitigation strategy which restricts heavy goods vehicles (HGV) entering the city during the daytime (7:00 a.m.–10:00 p.m.). The restrictions cause a large influx of high PM emitting HGVs into the city at a time when the PBL is particularly low, which causes PM₁₀ concentrations to be accentuated. It is suggested that changing the HGV restriction times to allow access in the middle of the day might be beneficial to reduce PM₁₀ concentrations. However, further studies are required to evaluate the resultant effect on congestion and human exposure.

Author contributions

JMC, BL, CD and EN analysed the filters using offline-AMS. TKM, SKS, BRG conducted the filter sampling and measurements of OC/EC, WSOC and elements. JMC developed the offline-AMS method and was supervised by BL, MRH and EN. JMC, BL, CD, MRH and EN contributed to data interpretation. All authors contributed to the discussion, writing and editing of the article.

Declaration of competing interest

The authors declare that they have no known competing financial interests or personal relationships that could have appeared to influence the work reported in this paper.

Data availability

Data will be made available on request.

Acknowledgements

This work was supported by UK NERC project DelhiFlux under the Newton Bhabha Fund programme Air Pollution and Human Health in a Developing Megacities (APHH-India), NERC reference numbers NE/P016502/1 and NE/P016472/1. This work was also supported by the Earth System Science Organization, Ministry of Earth Sciences, Government of India, under the Indo-UK joint collaboration grant no. MoES/16/19/2017-APHH (DelhiFlux). A NERC E3 DTP studentship supported James M. Cash (NE/L002558/1). The NERC National Capability award SUNRISE (NE/R000131/1) also supported these measurements. We thank the Director of CSIR-National Physical Laboratory for allowing us to carry out this research.

Appendix A. Supplementary data

Supplementary data to this article can be found online at <https://doi.org/10.1016/j.atmosenv.2023.120123>.

References

- Allan, J.D., Jimenez, J.L., Williams, P.I., Alfarra, M.R., Bower, K.N., Jayne, J.T., Coe, H., Worsnop, D.R., 2003. Quantitative sampling using an Aerodyne aerosol mass spectrometer 1. Techniques of data interpretation and error analysis. *J. Geophys. Res. Atmos.* 108 <https://doi.org/10.1029/2002JD002358>.
- Banoo, R., Sharma, S.K., Gadi, R., Gupta, S., Mandal, T.K., 2020. Seasonal variation of carbonaceous species of PM10 over urban sites of national capital region of India. *Aerosol Sci. Eng.* 4, 111–123. <https://doi.org/10.1007/s41810-020-00058-2>.
- Bottenus, C.L.H., Massoli, P., Sueper, D., Canagaratna, M.R., Vanderschelden, G., Jobson, B.T., VanReken, T.M., 2018. Identification of amines in wintertime ambient particulate material using high resolution aerosol mass spectrometry. *Atmos. Environ.* 180, 173–183. <https://doi.org/10.1016/j.atmosenv.2018.01.044>.
- Bozzetti, C., Sosedova, Y., Xiao, M., Daellenbach, K.R., Ulevicius, V., Dudoitis, V., Mordas, G., Byćenkiene, S., Plauskaitė, K., Vlachou, A., Golly, B., Chazeau, B., Besombes, J.-L., Baltensperger, U., Jaffrezo, J.-L., Slowik, J.G., El Haddad, I., Prévôt, A.S.H., 2017. Argon offline-AMS source apportionment of organic aerosol over yearly cycles for an urban, rural, and marine site in northern Europe. *Atmos. Chem. Phys.* 17, 117–141. <https://doi.org/10.5194/acp-17-117-2017>.
- Canagaratna, M.R., Jayne, J.T., Jimenez, J.L., Allan, J.D., Alfarra, M.R., Zhang, Q., Onasch, T.B., Drewnick, F., Coe, H., Middlebrook, A., Delia, A., Williams, L.R., Trimborn, A.M., Northway, M.J., DeCarlo, P.F., Kolb, C.E., Davidovits, P., Worsnop, D.R., 2007. Chemical and microphysical characterization of ambient aerosols with the aerodyne aerosol mass spectrometer. *Mass Spectrom. Rev.* 26, 185–222. <https://doi.org/10.1002/mas.20115>.
- Cash, J.M., Langford, B., Di Marco, C., Mullinger, N.J., Allan, J., Reyes-Villegas, E., Joshi, R., Heal, M.R., Acton, W.J.F., Hewitt, C.N., Misztal, P.K., Drysdale, W., Mandal, T.K., Gadi, R., Gurjar, B.R., Nemitz, E., 2021. Seasonal analysis of submicron aerosol in Old Delhi using high-resolution aerosol mass spectrometry: chemical characterisation, source apportionment and new marker identification. *Atmos. Chem. Phys.* 21, 10133–10158. <https://doi.org/10.5194/acp-21-10133-2021>.
- Chen, Q., Ikemori, F., Higo, H., Asakawa, D., Mochida, M., 2016. Chemical structural characteristics of HULIS and other fractionated organic matter in urban aerosols: results from mass spectral and FT-IR analysis. *Environ. Sci. Technol.* 4, 1721–1730. <https://doi.org/10.1021/acs.est.5b05277>.
- Chow, J.C., Watson, J.G., Chen, L.W.A., Arnott, W.P., Moosmüller, H., Fung, K., 2004. Equivalence of elemental carbon by thermal/optical reflectance and transmittance with different temperature protocols. *Environ. Sci. Technol.* 38, 4414–4422. <https://doi.org/10.1021/es034936u>.
- Chowdhury, S., Dey, S., Tripathi, S.N., Beig, G., Mishra, A.K., Sharma, S., 2017. “Traffic intervention” policy fails to mitigate air pollution in megacity Delhi. *Environ. Sci. Technol.* 51, 8–13. <https://doi.org/10.1016/j.envsci.2017.04.018>.
- Daellenbach, K.R., Bozzetti, C., Křepelová, A., Canonaco, F., Wolf, R., Zotter, P., Fermo, P., Crippa, M., Slowik, J.G., Sosedova, Y., Zhang, Y., Huang, R., Poulain, L., Szidat, S., Baltensperger, U., El Haddad, I., H. Prévôt, A.S., To, C., H. Prévôt, A.S., 2016. Characterization and source apportionment of organic aerosol using offline aerosol mass spectrometry. *Atmos. Meas. Tech.* 9, 8599–8644. <https://doi.org/10.5194/amt-9-23-2016>.
- Daellenbach, K.R., Stefanelli, G., Bozzetti, C., Vlachou, A., Fermo, P., Gonzalez, R., Piazzalunga, A., Colombi, C., Canonaco, F., Hueglin, C., Kasper-Giehl, A., Jaffrezo, J.-L., Bianchi, F., Slowik, J.G., Baltensperger, U., El Haddad, I., Prévôt, A.S.H., 2017. Long-term chemical analysis and organic aerosol source apportionment at 9 sites in Central Europe: source identification and uncertainty assessment. *Atmos. Chem. Phys. Discuss.* 17, 13265–13282. <https://doi.org/10.5194/acp-2017-124>.
- DeCarlo, P.F., Kimmel, J.R., Trimborn, A., Northway, M.J., Jayne, J.T., Aiken, A.C., Gonin, M., Fuhrer, K., Horvath, T., Docherty, K.S., Worsnop, D.R., Jimenez, J.L., 2006. Field-deployable, high-resolution, time-of-flight aerosol mass spectrometer. *Anal. Chem.* 78, 8281–8289. <https://doi.org/10.1021/ac061249n>.
- Denier van der Gon, H.A.C., Hulskotte, J.H.J., Visschedijk, A.J.H., Schaap, M., 2007. A revised estimate of copper emissions from road transport in UNECE-Europe and its impact on predicted copper concentrations. *Atmos. Environ.* 41, 8697–8710. <https://doi.org/10.1016/j.atmosenv.2007.07.033>.
- Docherty, K.S., Aiken, A.C., Huffman, J.A., Ulbrich, I.M., Decarlo, P.F., Sueper, D., Worsnop, D.R., Snyder, D.C., Peltier, R.E., Weber, R.J., Grover, B.D., Eatough, D.J., Williams, B.J., Goldstein, A.H., Ziemann, P.J., Jimenez, J.L., 2011. The 2005 study of organic aerosols at riverside (SOAR-1): instrumental intercomparisons and fine particle composition. *Atmos. Chem. Phys.* 11, 12387–12420. <https://doi.org/10.5194/acp-11-12387-2011>.
- Duplissy, J., De Carlo, P.F., Dommen, J., Alfarra, M.R., Metzger, A., Barmpadimos, I., Prevot, A.S.H., Weingartner, E., Tritscher, T., Gysel, M., Aiken, A.C., Jimenez, J.L., Canagaratna, M.R., Worsnop, D.R., Collins, D.R., Tomlinson, J., Baltensperger, U., 2011. Relating hygroscopicity and composition of organic aerosol particulate matter. *Atmos. Chem. Phys.* 11, 1155–1165. <https://doi.org/10.5194/acp-11-1155-2011>.
- Gao, Z.-F., Long, H.-M., Dai, B., Gao, X.-P., 2019. Investigation of reducing particulate matter (PM) and heavy metals pollution by adding a novel additive from metallurgical dust (MD) during coal combustion. *J. Hazard. Mater.* 373, 335–346. <https://doi.org/10.1016/j.jhazmat.2019.03.057>.
- Ge, X., Li, L., Chen, Y., Chen, H., Wu, D., Wang, J., Xie, X., Ge, S., Ye, Z., Xu, J., Chen, M., 2017. Aerosol characteristics and sources in Yangzhou, China resolved by offline aerosol mass spectrometry and other techniques. *Environ. Pollut.* 225, 74–85. <https://doi.org/10.1016/j.envpol.2017.03.044>.
- Goel, R., Guttikunda, S.K., 2015. Evolution of on-road vehicle exhaust emissions in Delhi. *Atmos. Environ.* 105, 78–90. <https://doi.org/10.1016/j.atmosenv.2015.01.045>.
- Gohlke, R.S., McLafferty, F.W., 1962. Mass spectrometric analysis: aliphatic amines. *Anal. Chem.* 34, 1281–1287. <https://doi.org/10.1021/ac60190a025>.
- Goyal, P., Gulia, S., Goyal, S.K., Kumar, R., 2019. Assessment of the effectiveness of policy interventions for air quality control regions in Delhi city. *Environ. Sci. Pollut. Res.* 26, 30967–30979. <https://doi.org/10.1007/s11356-019-06236-1>.
- Gulia, S., Mittal, A., Khare, M., 2018. Quantitative evaluation of source interventions for urban air quality improvement - a case study of Delhi city. *Atmos. Pollut. Res.* 9, 577–583. <https://doi.org/10.1016/j.apr.2017.12.003>.
- Gulia, S., Shukla, N., Padhi, L., Bosu, P., Goyal, S.K., Kumar, R., 2022. Evolution of air pollution management policies and related research in India. *Environ. Challenges* 6, 100431. <https://doi.org/10.1016/j.envc.2021.100431>.
- Han, Y., Kawamura, K., Chen, Q., Mochida, M., 2016. Formation of high-molecular-weight compounds via the heterogeneous reactions of gaseous C8-C10n-aldehydes in the presence of atmospheric aerosol components. *Atmos. Environ.* 126, 290–297. <https://doi.org/10.1016/j.atmosenv.2015.11.050>.
- Harrison, R.M., Allan, J., Carruthers, D., Heal, M.R., Lewis, A.C., Marnner, B., Murrells, T., Williams, A., 2021. Non-exhaust vehicle emissions of particulate matter and VOC from road traffic: a review. *Atmos. Environ.* 262, 118592. <https://doi.org/10.1016/j.atmosenv.2021.118592>.
- Herring, C.L., Faiola, C.L., Massoli, P., Sueper, D., Erickson, M.H., McDonald, J.D., Simpson, C.D., Yost, M.G., Jobson, B.T., Van Reken, T.M., 2015. New methodology for quantifying polycyclic aromatic hydrocarbons (PAHs) using high-resolution aerosol mass spectrometry. *Aerosol Sci. Technol.* 49, 1131–1148. <https://doi.org/10.1080/02786826.2015.1101050>.
- Hunt, A.L., Petrucci, G.A., 2002. Analysis of ultrafine and organic particles by aerosol mass spectrometry. *TrAC - Trends Anal. Chem.* 21, 74–81. [https://doi.org/10.1016/S0165-9936\(01\)00138-8](https://doi.org/10.1016/S0165-9936(01)00138-8).
- Jain, S., Sharma, S.K., Vijayan, N., Mandal, T.K., 2020. Seasonal characteristics of aerosols (PM2.5 and PM10) and their source apportionment using PMF: a four year study over Delhi, India. *Environ. Pollut.* 262, 114337. <https://doi.org/10.1016/j.envpol.2020.114337>.
- Jayarathne, T., Stockwell, C.E., Christian, T.J., Bhawe, P.V., Praveen, P.S., Panday, A.K., Adhikari, S., Maharjan, R., Goetz, J.D., DeCarlo, P.F., Saikawa, E., Yokelson, R.J., Stone, E.A., 2017. Nepal Ambient Monitoring and Source Testing Experiment (NAMASTE): emissions of particulate matter from wood and dung cooking fires, brick kilns, generators, trash and crop residue burning. Submitted 2259–2286.
- Jayarathne, T., Stockwell, C.E., Gilbert, A.A., Daugherty, K., Cochrane, M.A., Ryan, K.C., Putra, E.I., Saharjo, B.H., Nurhayati, A.D., Albar, I., Yokelson, R.J., Stone, E.A., 2018. Chemical characterization of fine particulate matter emitted by peat fires in Central Kalimantan, Indonesia, during the 2015 El Niño. *Atmos. Chem. Phys.* 18, 2585–2600. <https://doi.org/10.5194/acp-18-2585-2018>.
- Jonidi Jafari, A., Charkhloo, E., Pasalari, H., 2021. Urban air pollution control policies and strategies: a systematic review. *J. Environ. Heal. Sci. Eng.* 19, 1911–1940. <https://doi.org/10.1007/s40201-021-00744-4>.
- Kathuria, V., 2005. Vehicular pollution control in Delhi: impact of compressed natural gas. *Econ. Polit. Wkly.* 40, 1907–1916.
- Keene, W.C., Lobert, J.M., Crutzen, P.J., Maben, J.R., Scharffe, D.H., Landmann, T., Hély, C., Brain, C., 2006. Emissions of major gaseous and particulate species during experimental burns of southern African biomass. *J. Geophys. Res. Atmos.* 111. <https://doi.org/10.1029/2005JD006319>.
- Khillare, P.S., Balachandran, S., Meena, B.R., 2004. Spatial and temporal variation of heavy metals in atmospheric aerosol of Delhi. *Environ. Monit. Assess.* 90, 1–21. <https://doi.org/10.1023/B:EMAS.0000003555.36394.17>.
- Kothai, P., Saradhi, I.V., Prathibha, P., Hopke, P.K., Pandit, G.G., Puranik, V.D., 2008. Source apportionment of coarse and fine particulate matter at Navi Mumbai, India. *Aerosol Air Qual. Res.* 8, 423–436. <https://doi.org/10.4209/aaqr.2008.07.0027>.

- Krelling, C., Badami, M.G., 2022. Cost-effectiveness analysis of compressed natural gas implementation in the public bus transit fleet in Delhi, India. *Transp. Policy* 115, 49–61. <https://doi.org/10.1016/j.tranpol.2021.10.019>.
- Li, Y.-C., Shu, M., Ho, S.S.H., Wang, C., Cao, J.-J., Wang, G.-H., Wang, X.-X., Wang, K., Zhao, X.-Q., 2015. Characteristics of PM_{2.5} emitted from different cooking activities in China. *Atmos. Res.* 166, 83–91. <https://doi.org/10.1016/j.atmosres.2015.06.010>.
- Li, Z., Wang, Q., Xiao, Z., Fan, L., Wang, D., Li, X., Du, J., Cheng, J., 2020. Behaviors of chromium in coal-fired power plants and associated atmospheric emissions in guizhou, southwest China. *Atmosphere (Basel)* 11. <https://doi.org/10.3390/atmos11090951>.
- Lin, C., Ceburnis, D., Huang, R.J., Xu, W., Spohn, T., Martin, D., Buckley, P., Wenger, J., Hellebust, S., Rinaldi, M., Cristina Facchini, M., O'Dowd, C., Ovadnevaite, J., 2019. Wintertime aerosol dominated by solid-fuel-burning emissions across Ireland: insight into the spatial and chemical variation in submicron aerosol. *Atmos. Chem. Phys.* 19, 14091–14106. <https://doi.org/10.5194/acp-19-14091-2019>.
- McLafferty, W.F., Turecek, F., 1993. Interpretation of Mass Spectra. University Science Books, Sausalito, CA. <https://doi.org/10.1016/b978-012483385-2/50003-8>.
- Mihara, T., Mochida, M., 2011. Characterization of solvent-extractable organics in urban aerosols based on mass spectrum analysis and hygroscopic growth measurement. *Environ. Sci. Technol.* 45, 9168–9174. <https://doi.org/10.1021/es201271w>.
- Mohr, C., DeCarlo, P.F., Hering, M.F., Chirico, R., Slowik, J.G., Richter, R., Reche, C., Alastuey, A., Querol, X., Seco, R., Peñuelas, J., Jiménez, J.L., Crippa, M., Zimmermann, R., Baltensperger, U., Prévôt, A.S.H., 2012. Identification and quantification of organic aerosol from cooking and other sources in Barcelona using aerosol mass spectrometer data. *Atmos. Chem. Phys.* 12, 1649–1665. <https://doi.org/10.5194/acp-12-1649-2012>.
- Montes, C., Sapkota, T., Singh, B., 2022. Seasonal patterns in rice and wheat residue burning and surface PM_{2.5} concentration in northern India. *Atmos. Environ.* X 13, 100154. <https://doi.org/10.1016/j.aeoaa.2022.100154>.
- Nakoudi, K., Giannakaki, E., Dandou, A., Tombrou, M., Kompula, M., 2018. Planetary boundary layer variability over New Delhi, India, during EUCAARI project. *Atmos. Meas. Tech. Discuss.* 1–33. <https://doi.org/10.5194/amt-2018-342>.
- Negi, A., Kumar, A., 2019. Long-term electricity demand scenarios for India: implications of energy efficiency. In: 2018 Int. Conf. Power Energy, Environ. Intell. Control. PEEIC 2018, pp. 462–467. <https://doi.org/10.1109/PEEIC.2018.8665452>.
- Paatero, P., 1999. The multilinear engine—a table-driven, least squares program for solving multilinear problems, including the n-way parallel factor analysis model. *J. Comput. Graph. Stat.* 8, 854–888. <https://doi.org/10.1080/10618600.1999.10474853>.
- Paatero, P., Hopke, P.K., 2003. Discarding or downweighting high-noise variables in factor analytic models. *Anal. Chim. Acta* 490, 277–289. [https://doi.org/10.1016/S0003-2670\(02\)01643-4](https://doi.org/10.1016/S0003-2670(02)01643-4).
- Paatero, P., Tapper, U., 1994. Positive matrix factorization: a non-negative factor model with optimal utilization of error estimates of data values. *Environmetrics* 5, 111–126. <https://doi.org/10.1002/env.3170050203>.
- Pacyna, E.G., Pacyna, J.M., Fudala, J., Strzelecka-Jastrzab, E., Hlawiczka, S., Panasiuk, D., Nitter, S., Peggler, T., Pfeiffer, H., Friedrich, R., 2007. Current and future emissions of selected heavy metals to the atmosphere from anthropogenic sources in Europe. *Atmos. Environ.* 41, 8557–8566. <https://doi.org/10.1016/j.atmosenv.2007.07.040>.
- Pandey, A., Brauer, M., Cropper, M.L., Balakrishnan, K., Mathur, P., Dey, Sagnik, Turkuglu, B., Kumar, G.A., Khare, M., Beig, G., Gupta, T., Krishnankutty, R.P., Causey, K., Cohen, A.J., Bhargava, S., Aggarwal, A.N., Agrawal, A., Awasthi, S., Bennitt, F., Bhagwat, S., Bhanumati, P., Burkart, K., Chakma, J.K., Chiles, T.C., Chowdhury, S., Christopher, D.J., Dey, Subhojit, Fisher, S., Fraumeni, B., Fuller, R., Ghoshal, A.G., Golechha, M.J., Gupta, P.C., Gupta, Rachita, Gupta, Rajeev, Gupta, S., Gutikunda, S., Hanrahan, D., Harikrishnan, S., Jeemon, P., Joshi, T.K., Kant, R., Kant, S., Kaur, T., Koul, P.A., Kumar, Praveen, Kumar, R., Larson, S.L., Lodha, R., Madhipatla, K.K., Mahesh, P.A., Malhotra, R., Managi, S., Martin, K., Mathai, M., Mathew, J.L., Mehrotra, R., Mohan, B.V.M., Mohan, V., Mukhopadhyay, S., Mutreja, P., Naik, N., Nair, S., Pandian, J.D., Pant, P., Perianayagam, A., Prabhakaran, D., Prabhakaran, P., Rath, G.K., Ravi, S., Roy, A., Sabde, Y.D., Salvi, S., Sambandam, S., Sharma, B., Sharma, M., Sharma, S., Sharma, R.S., Shrivastava, A., Singh, S., Singh, V., Smith, R., Stanaway, J.D., Taghian, G., Tandon, N., Thakur, J.S., Thomas, N.J., Toteja, G.S., Varghese, C.M., Venkataraman, C., Venugopal, K.N., Walker, K.D., Watson, A.Y., Wozniak, S., Xavier, D., Yadama, G.N., Yadav, G., Shukla, D.K., Bekedam, H.J., Reddy, K.S., Guleria, R., Vos, T., Lim, S.S., Dandona, R., Kumar, S., Kumar, Pushpam, Landrigan, P.J., Dandona, L., 2021. Health and economic impact of air pollution in the states of India: the Global Burden of Disease Study 2019. *Lancet Planet. Heal.* 5, e25–e38. [https://doi.org/10.1016/S2542-5196\(20\)30298-9](https://doi.org/10.1016/S2542-5196(20)30298-9).
- Pervez, S., Verma, M., Tiwari, S., Chakrabarty, R.K., Watson, J.G., Chow, J.C., Panicker, A.S., Deb, M.K., Siddiqui, M.N., Pervez, Y.F., 2019. Household solid fuel burning emission characterization and activity levels in India. *Sci. Total Environ.* 654, 493–504. <https://doi.org/10.1016/j.scitotenv.2018.11.019>.
- Pieber, S.M., El Haddad, I., Slowik, J.G., Canagaratna, M.R., Jayne, J.T., Platt, S.M., Bozzetti, C., Daellenbach, K.R., Fröhlich, R., Vlachou, A., Klein, F., Dommen, J., Miljevic, B., Jiménez, J.L., Worsnop, D.R., Baltensperger, U., Prévôt, A.S.H., 2016. Inorganic salt interference on CO₂+ in aerodyne AMS and ACSM organic aerosol composition studies. *Environ. Sci. Technol.* 50, 10494–10503. <https://doi.org/10.1021/acs.est.6b01035>.
- Reizer, M., Juda-Rezler, K., 2016. Explaining the high PM₁₀ concentrations observed in Polish urban areas. *Air Qual. Atmos. Heal.* 9, 517–531. <https://doi.org/10.1007/s11869-015-0358-z>.
- Reyes-Villegas, E., Panda, U., Darbyshire, E., Cash, J.M., Joshi, R., Langford, B., Di Marco, C.F., Mullinger, N., Acton, W.J.F., Drysdale, W., Nemitz, E., Flynn, M., Voliotis, A., McFiggans, G., Coe, H., Lee, J., Hewitt, C.N., Heal, M.R., Gunthe, S.S., Shivani, Gadi, R., Singh, S., Soni, V., Allan, J.D., 2020. PM₁ composition and source apportionment at two sites in Delhi, India across multiple seasons. *Atmos. Chem. Phys. Discuss.* 2020, 1–19. <https://doi.org/10.5194/acp-2020-894>.
- Saarikoski, S., Timonen, H., Saarnio, K., Aurela, M., Järvi, L., Keronen, P., Kerminen, V.-M., Hillamo, R., 2008. Sources of organic carbon in fine particulate matter in northern European urban air. *Atmos. Chem. Phys.* 8, 6281–6295.
- Sharma, S.K., Agarwal, P., Mandal, T.K., Karapurkar, S.G., Shenoy, D.M., Peshin, S.K., Gupta, A., Saxena, M., Jain, S., Sharma, A., Saraswati, 2017. Study on ambient air quality of megacity Delhi, India during odd-even strategy. *Mapan* 32, 155–165. <https://doi.org/10.1007/s12647-016-0201-5>.
- Sharma, S.K., Banoo, R., Mandal, T.K., 2021. Seasonal characteristics and sources of carbonaceous components and elements of PM₁₀ (2010–2019) in Delhi, India. *J. Atmos. Chem.* 78, 251–270. <https://doi.org/10.1007/s10874-021-09424-x>.
- Sharma, S.K., Mandal, T.K., Saxena, M., Rashmi, Rohtash, Sharma, A., Gautam, R., 2014. Source apportionment of PM₁₀ by using positive matrix factorization at an urban site of Delhi, India. *Urban Clim* 10, 656–670. <https://doi.org/10.1016/j.uclim.2013.11.002>.
- Sharma, S.K., Mandal, T.K., Sharma, A., Sarawati, Jain, S., 2018. Seasonal and annual trends of carbonaceous species of PM₁₀ over a megacity Delhi, India during 2010–2017. *J. Atmos. Chem.* 75, 305–318. <https://doi.org/10.1007/s10874-018-9379-y>.
- Sindhvani, R., Goyal, P., 2014. Assessment of traffic-generated gaseous and particulate matter emissions and trends over Delhi (2000–2010). *Atmos. Pollut. Res.* 5, 438–446. <https://doi.org/10.5094/APR.2014.051>.
- Singh, V., Biswal, A., Kesarkar, A.P., Mor, S., Ravindra, K., 2020. High resolution vehicular PM₁₀ emissions over megacity Delhi: relative contributions of exhaust and non-exhaust sources. *Sci. Total Environ.* 699, 134273. <https://doi.org/10.1016/j.scitotenv.2019.134273>.
- Singh, V., Sahu, S.K., Kesarkar, A.P., Biswal, A., 2018. Estimation of high resolution emissions from road transport sector in a megacity Delhi. *Urban Clim* 26, 109–120. <https://doi.org/10.1016/j.uclim.2018.08.011>.
- Stewart, G.J., Acton, W.J.F., Nelson, B.S., Vaughan, A.R., Hopkins, J.R., Arya, R., Mondal, A., Jangirh, R., Ahlawat, S., Yadav, L., Sharma, S.K., Dunmore, R.E., Yunus, S.S.M., Nicholas Hewitt, C., Nemitz, E., Mullinger, N., Gadi, R., Sahu, L.K., Tripathi, N., Rickard, A.R., Lee, J.D., Mandal, T.K., Hamilton, J.F., 2021. Emissions of non-methane volatile organic compounds from combustion of domestic fuels in Delhi, India. *Atmos. Chem. Phys.* 21, 2383–2406. <https://doi.org/10.5194/acp-21-2383-2021>.
- Sun, Y., Du, W., Fu, P., Wang, Q., Li, J., Ge, X., Zhang, Q., Zhu, C., Ren, L., Xu, W., Zhao, J., Han, T., Worsnop, D.R., Wang, Z., 2016. Primary and secondary aerosols in Beijing in winter: sources, variations and processes. *Atmos. Chem. Phys.* 16, 8309–8329. <https://doi.org/10.5194/acp-16-8309-2016>.
- Sun, Y., Zhang, Q., Zheng, M., Ding, X., Edgerton, E.S., Wang, X., 2011. Characterization and source apportionment of water-soluble organic matter in atmospheric fine particles (PM_{2.5}) with high-resolution aerosol mass spectrometry and GC-MS. *Environ. Sci. Technol.* 45, 4854–4861. <https://doi.org/10.1021/es200162h>.
- Suneja, J., Kotnala, G., Kaur, A., Mandal, T.K., Sharma, S.K., 2020. Long-Term measurements of SO₂ over Delhi, India. *Mapan* 35, 125–133. <https://doi.org/10.1007/s12647-019-00349-1>.
- Tang, Q., Du, C., Liu, J., Fan, L., Niu, J., Miao, C., Li, W., Fu, B., 2022. The retention and speciation transformation mechanisms of chromium during bituminous coal combustion: effects of inorganic minerals and combustion temperature. *Fuel Process. Technol.* 232, 107273. <https://doi.org/10.1016/j.fuproc.2022.107273>.
- Ulbrich, I.M., Canagaratna, M.R., Zhang, Q., Worsnop, D.R., Jimenez, J.L., 2009. Interpretation of organic components from Positive Matrix Factorization of aerosol mass spectrometric data. *Atmos. Chem. Phys.* 9, 2891–2918. <https://doi.org/10.5194/acp-9-2891-2009>.
- Wang, L., Slowik, J.G., Tripathi, N., Bhattu, D., Rai, P., Kumar, V., Vats, P., Satish, R., Baltensperger, U., Ganguly, D., Rastogi, N., Sahu, L.K., Tripathi, S.N., Prévôt, A.S.H., 2020. Source characterization of volatile organic compounds measured by proton-transfer-reaction time-of-flight mass spectrometers in Delhi, India. *Atmos. Chem. Phys.* 20, 9753–9770. <https://doi.org/10.5194/acp-20-9753-2020>.
- Xu, J., Shi, J., Zhang, Q., Ge, X., Canonaco, F., Prévôt, A.S.H., Vonwiller, M., Szidat, S., Ge, J., Ma, J., An, Y., Kang, S., Qin, D., 2016. Wintertime organic and inorganic aerosols in Lanzhou, China: sources, processes, and comparison with the results during summer. *Atmos. Chem. Phys.* 16, 14937–14957. <https://doi.org/10.5194/acp-16-14937-2016>.
- Yang, J., Urpelainen, J., 2019. The future of India's coal-fired power generation capacity. *J. Clean. Prod.* 226, 904–912. <https://doi.org/10.1016/j.jclepro.2019.04.074>.
- Ye, Z., Liu, J., Gu, A., Feng, F., Liu, Y., Bi, C., Xu, J., Li, L., Chen, H., Chen, Y., Dai, L., Zhou, Q., Ge, X., 2017. Chemical characterization of fine particulate matter in Changzhou, China, and source apportionment with offline aerosol mass spectrometry. *Atmos. Chem. Phys.* 17, 2573–2592. <https://doi.org/10.5194/acp-17-2573-2017>.